PHYSICAL REVIEW B **83**, 104506 (2011)

Stripe order in superconducting $La_{2-x}Ba_xCuO_4$ ($0.095 \leqslant x \leqslant 0.155$)

M. Hücker,[1] M. v. Zimmermann,[2] G. D. Gu,[1] Z. J. Xu,[1] J. S. Wen,[1] Guangyong Xu,[1] H. J. Kang,[3,*] A. Zheludev,[4,†] and J. M. Tranquada[1]

[1]*Condensed Matter Physics & Materials Science Department, Brookhaven National Laboratory, Upton, New York 11973, USA*
[2]*Hamburger Synchrotronstrahlungslabor at Deutsches Elektronen-Synchrotron DESY, D-22603 Hamburg, Germany*
[3]*NIST Center for Neutron Research, National Institute of Standards and Technology, Gaithersburg, Maryland 20899, USA*
[4]*Neutron Scattering Science Division, Oak Ridge National Laboratory, Oak Ridge, Tennessee 37831, USA*

(Received 27 May 2010; revised manuscript received 23 September 2010; published 17 March 2011)

The correlations between stripe order, superconductivity, and crystal structure in $La_{2-x}Ba_xCuO_4$ single crystals have been studied by means of x-ray and neutron diffraction as well as static magnetization measurements. The derived phase diagram shows that charge stripe order (CO) coexists with bulk superconductivity in a broad range of doping around $x = 1/8$, although the CO order parameter and correlation length fall off quickly for $x \neq 1/8$. Except for $x = 0.155$, the onset of CO always coincides with the transition between the orthorhombic and the tetragonal or less orthorhombic low-temperature structures. The CO transition evolves from a sharp drop at low x to a more gradual transition at higher x, eventually falling below the structural phase boundary for optimum doping. With respect to the interlayer CO correlations, we find no qualitative change of the stripe stacking order as a function of doping, and in-plane and out-of-plane correlations disappear simultaneously at the transition. Similarly to the CO, the spin stripe order (SO) is also most pronounced at $x = 1/8$. Truly static SO sets in below the CO and coincides with the first appearance of in-plane superconducting correlations at temperatures significantly above the bulk transition to superconductivity (SC). Indications that bulk SC causes a reduction of the spin or charge stripe order could not be identified. We argue that CO is the dominant order that is compatible with SC pairing but competes with SC phase coherence. Comparing our results with data from the literature, we find good agreement if all results are plotted as a function of x' instead of the nominal x, where x' represents an estimate of the actual Ba content, extracted from the doping dependence of the structural transition between the orthorhombic phase and the tetragonal high-temperature phase.

DOI: 10.1103/PhysRevB.83.104506 PACS number(s): 74.72.−h, 71.45.Lr, 74.25.Dw

I. INTRODUCTION

The prototypical high-temperature superconductor[1] $La_{2-x}Ba_xCuO_4$ is particularly well known for its unique doping dependence of the bulk superconducting (SC) phase.[2] While its sister compound $La_{2-x}Sr_xCuO_4$, as most other high-temperature superconductors, displays a dome-shaped SC phase boundary $T_c(x)$,[3,4] in the Ba-based compound $T_c(x)$ shows a deep depression centered at $x = 1/8$.[2,5] It was discovered early on that the so-called 1/8 anomaly is accompanied by a structural transition from low-temperature orthorhombic (LTO) to low-temperature tetragonal (LTT) symmetry,[6,7] not observed in pure $La_{2-x}Sr_xCuO_4$, and that bulk SC is replaced by some kind of antiferromagnetic (AF) order.[8–11] The complex nature of the magnetic phase was first identified by neutron and x-ray diffraction experiments for an analogous phase in $La_{1.6-x}Nd_{0.4}Sr_xCuO_4$,[12–15] and later on confirmed in $La_{1.875}Ba_{0.125-y}Sr_yCuO_4$,[16,17] $La_{1.875}Ba_{0.125}CuO_4$,[18–20] and $La_{1.8-x}Eu_{0.2}Sr_xCuO_4$.[21,22] Undoped ($x = 0$), all of these compounds are quasi-two-dimensional commensurate spin $S = 1/2$ Heisenberg AF.[23–25] But doped with sufficient charge carriers, they exhibit incommensurate nuclear and magnetic superstructure reflections (which we will describe below). Among the debated interpretations is the so-called stripe model in which the charge carriers in the CuO_2 planes segregate into hole-rich stripes, thus forming antiphase boundaries between intermediate spin stripes with locally AF correlations.[12,26–28] In the LTT phase, which breaks the fourfold rotational symmetry of the individual CuO_2 planes, the electron-lattice coupling is believed to play a central role in the pinning of stripes,[29–33] although recent experiments under pressure revealed that stripes can break the symmetry even in the absence of long-range LTT order.[34]

So far, $La_{1.6-x}Nd_{0.4}Sr_xCuO_4$ is the only system with a stripe-ordered LTT phase, where magnetic *and* charge order have been studied with diffraction on *both* sides of $x = 1/8$.[15] The results were interpreted as indicating that local magnetic order rather than charge stripe order is responsible for the suppression of bulk SC, and that charge stripes are compatible with SC as long as the magnetic correlations remain dynamic. More recent experimental and theoretical results on $La_{1.875}Ba_{0.125}CuO_4$ support the revised view that, in principle, static spin and charge stripes are compatible with SC pairing, but, owing to their orthogonal arrangement in adjacent planes, they compete with superconducting phase order.[35–38]

It is desirable to analyze $La_{2-x}Ba_xCuO_4$ in a broader range of doping to test the generality of the observations. This system has two advantages over rare-earth-doped $La_{2-x}Sr_xCuO_4$: First, only one element is substituted for La. Second, the Ba^{2+} ions are nonmagnetic, in contrast to, e.g., the Nd^{3+} ions, whose large magnetic moments interact with the spins of the Cu^{2+} ions in the CuO_2 planes.[39,40] Recent progress in the synthesis of $La_{2-x}Ba_xCuO_4$ single crystals with $x \leqslant 1/8$ has triggered numerous studies on the stripe order in the underdoped regime.[18–20,41–50]

Despite previous work, however, the doping dependence of many properties requires further clarification, such as the absolute intensities of the charge stripe order (CO) and spin

stripe order (SO) satellite reflections, the stripe correlations between the planes, the melting of the stripe order, and the compatibility with the generic stripe phase diagram. Furthermore, there is a great lack of information for $x > 1/8$ because crystal growth becomes progressively more challenging with increasing x.

These are the issues addressed in the present study on $La_{2-x}Ba_xCuO_4$ single crystals with $0.095 \leqslant x \leqslant 0.155$. We have characterized the CO with high-energy single-crystal x-ray diffraction (XRD), by probing the associated lattice modulation.[13,14,17] That a modulation of the electron density truly exists has been demonstrated previously in Ref. 19 for $La_{1.875}Ba_{0.125}CuO_4$ by means of resonant soft x-ray scattering. We have investigated the SO both in the traditional way, with neutron diffraction (ND), as well as in a less conventional way by tracing a recently identified weak ferromagnetic contribution to the normal state magnetic susceptibility.[51] The various structural phases have been studied mostly with XRD, and to some extent with ND, and the SC phase was analyzed with shielding and Meissner fraction measurements. As a result, we obtain the temperature versus Ba-concentration phase diagram displayed in Fig. 1. One of the key features is that CO exists over the entire range of x that we have studied, including the two bulk SC crystals with the lowest and highest x and maximum T_c on the order of 30 K. According to our quantitative analysis, the stripe order for these end compositions is already extremely weak, while it is most pronounced at $x = 1/8$. In the underdoped regime the CO

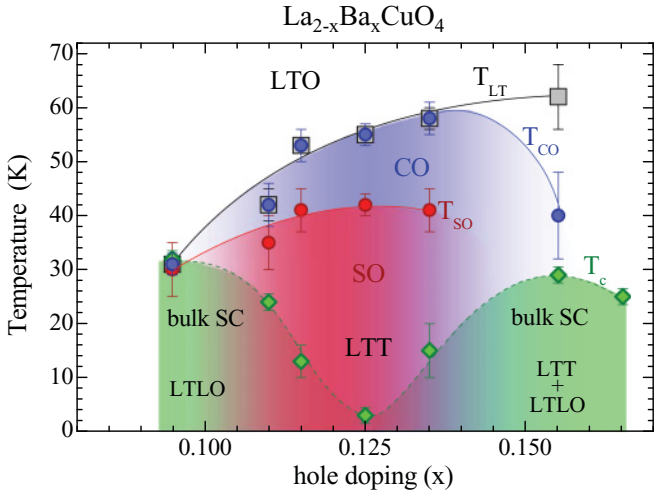

FIG. 1. (Color online) Temperature vs hole-doping phase diagram of $La_{2-x}Ba_xCuO_4$ single crystals. Onset temperatures: T_c of bulk superconductivity (SC), T_{CO} of charge stripe order (CO), T_{SO} of spin stripe order (SO), and T_{LT} of the low-temperature structural phases LTT and LTLO. At base temperature CO, SO, and SC coexist at least in the crystals with $0.095 \leqslant x \leqslant 0.135$. For $x = 0.155$ we identified CO but not SO, and observe a mixed LTT and LTLO phase. In the case of $x = 0.095$, very weak orthorhombic strain persists at low T. For $x = 0.165$ we have measured T_c only, before the crystal decomposed. Solid and dashed lines are guides to the eye. Although T_{CO}, T_{SO}, and T_{LT} for several x were also determined with XRD and ND, most data points in this figure are from magnetic susceptibility measurements. Here, only T_{SO} for $x = 0.095$ is from ND and T_{CO} and T_{LT} for $x = 0.155$ from XRD.

always disappears at the low-temperature structural transition, and for three crystals we can show that it melts isotropically. On the other hand, the onset of bulk SC left no noticeable mark in our CO and SO data.

The rest of the paper is organized as follows: In Sec. II we describe the experimental methods and the choice of reciprocal lattice used to index the reflections. In Sec. III we present four subsections dedicated to our results on crystal structure, CO, SO, and SC. In Sec. IV we summarize the doping dependence of the various properties as a function of the nominal and an estimated actual Ba content, compare our results with the literature, and in Sec. V finish with a short conclusion.

II. EXPERIMENTAL

A series of six $La_{2-x}Ba_xCuO_4$ single crystals with $0.095 \leqslant x \leqslant 0.155$ has been grown at Brookhaven with the traveling-solvent floating-zone method. Previously reported results on some of the compositions, in particular on the $x = 1/8$ crystal, have demonstrated a very high sample quality.[20,34–36,44,51–55] Because the compositions of the single crystals can deviate from their nominal stoichiometry (see Ref. 56), it has been vital to measure the structure, stripe order, and SC on pieces of the same crystal. In Fig. 2(a) we show the unit cell of the high-temperature tetragonal (HTT) phase, with space group $I4/mmm$. Although the supercells of the low-temperature phases LTO (space group $Bmab$) and LTT (space group $P4_2/ncm$) have a $\sqrt{2} \times \sqrt{2}$ larger basal plane rotated by 45°, we nevertheless specify the scattering vectors $\mathbf{Q} = (h,k,\ell)$ in all phases in units of $(2\pi/a_t, 2\pi/a_t, 2\pi/c)$ of the HTT cell with lattice parameters $a_t \simeq 3.78$ Å and $c \simeq 13.2$ Å.[57] In order to express the orthorhombic strain s in the LTO phase, we will refer to the lattice constants a_o and b_o of the LTO supercell, which are larger than a_t by a factor of $\sim\sqrt{2}$.

The XRD experiments were performed with the triple-axis diffractometer at wiggler beamline BW5 at DESY.[58] To create optimum conditions for studying the bulk properties in transmission geometry, most samples were disk shaped with a diameter (∼5 mm) significantly larger than the beam size of 1×1 mm^2, and a thickness (∼1 mm) close to the penetration depth of the 100 keV photons ($\lambda = 0.124$ Å). Counting rates are normalized to a storage ring current of 100 mA. To evaluate the x dependence of a superstructure reflection relative to $x = 0.125$, we have normalized its intensity with an integrated intensity ratio $I(0.125)/I(x)$ of a nearby fundamental Bragg reflection. For example, to normalize the (1,0,0) and $(2 + 2\delta,0,5.5)$ reflections, we have applied the factors $I_{(200)}(0.125)/I_{(200)}(x)$ and $I_{(206)}(0.125)/I_{(206)}(x)$ of the (2,0,0) and (2,0,6) Bragg reflections, respectively.

The ND data for $x = 0.115$, 0.125, and 0.135 were collected with the triple-axis spectrometer SPINS located at the NIST Center for Neutron Research using beam collimations of 55′-80′-S-80′-open (S = sample) with fixed final energy $E_f = 5$ meV. The $x = 0.095$ crystal was studied at triple-axis spectrometer HB-1 at the High Flux Isotope Reactor, Oak Ridge National Laboratory, using beam collimations of 48′-48′-S-40′-136′ with $E_f = 14.7$ meV. The cylindrical crystals, with a typical weight between 5 and 10 g, were mounted with their $(h,k,0)$ zone parallel to the scattering plane. Doping

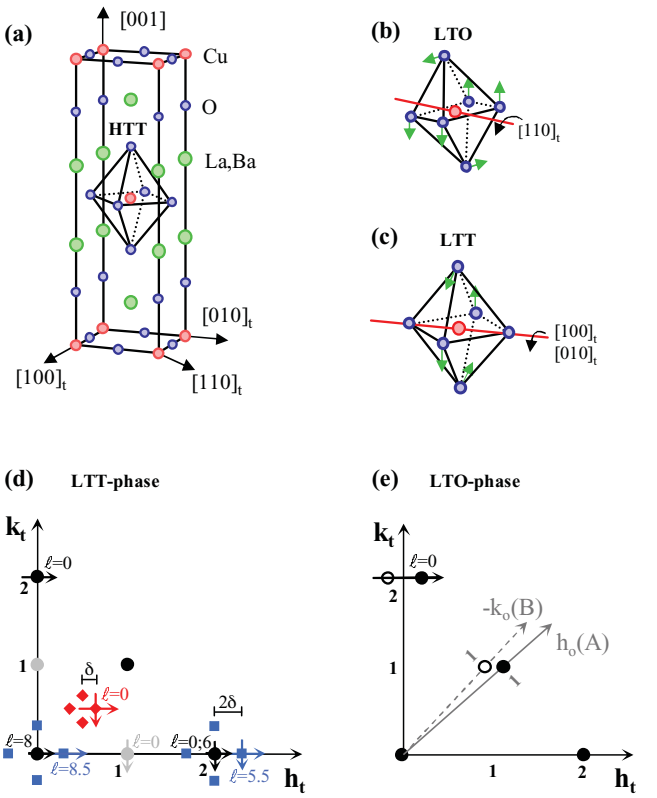

FIG. 2. (Color online) Crystal structure and reciprocal lattice of $La_{2-x}Ba_xCuO_4$. (a) Unit cell in the HTT phase (I_4/mmm). Tilt directions of the CuO_6 octahedra in (b) the LTO phase ($Bmab$) and (c) the LTT phase ($P4_2/ncm$). Note that in the LTT phase the tilt direction alternates between $[100]_t$ and $[010]_t$ in adjacent layers. The same is true for the stripe direction. Reciprocal lattice in terms of the HTT unit cell for (d) the LTT phase and (e) the LTO phase, projected along ℓ onto the (h,k) plane. Only reflections relevant to this work are shown. Fundamental Bragg reflections are indicated by black bullets and circles, CO reflections by blue squares, SO reflections by red diamonds, and superstructure reflections for $\ell = 0$ that are only allowed in the LTT and LTLO phases by gray bullets. In (e) we also indicate the reciprocal lattice of the orthorhombic phase with its two twin domains A (closed symbols) and B (open symbols). The trajectories of typical scans are indicated by arrows, along with the value of ℓ. The HTT phase compares to (d) with only the fundamental Bragg reflections present.

dependencies of intensities were obtained by normalizing the data with the irradiated sample volume.

The static magnetic susceptibility ($\chi = M/H$) measurements, used to study the stripe phase and the SC phase, were performed with a superconducting quantum interference device (SQUID) magnetometer for $H \parallel c$ and $H \parallel ab$. For these experiments crystal pieces with a typical weight of 0.5 g were used.

III. RESULTS

A. Crystal structure

Since the discovery of superconductivity in $La_{2-x}Ba_xCuO_4$ in the late 1980's,[1] the crystal structure, displayed in Fig. 2, has been studied intensively.[6] So far most diffraction results were obtained on polycrystals,[6,7,57] and only recently have single-crystal data been reported.[18,46,59] In the doping range considered here, $La_{2-x}Ba_xCuO_4$ undergoes two structural transitions with decreasing temperature: a second-order transition from HTT to LTO, and a first-order transition from LTO to another low-temperature phase that can either be LTT or the low-temperature less-orthorhombic (LTLO) phase (space group $Pccn$) that is a possible intermediate phase between LTO and LTT.[29] While the HTT phase is characterized by untilted CuO_6 octahedra forming flat CuO_2 planes, all low-temperature phases can be described by different patterns of tilted CuO_6 octahedra; see Figs. 2(a)–2(c).[29,57,60] In the LTO phase, the octahedra tilt by an angle Φ about the tetragonal $[1,1,0]_t$ axis that is diagonal to the CuO_2 square lattice and defines the orthorhombic $[1,0,0]_o$ axis [Fig. 2(b)]. In the LTT phase, the tilt axis runs parallel to the square lattice, but its direction alternates between $[1,0,0]_t$ and $[0,1,0]_t$ in adjacent planes.[6,12,57] In the LTLO phase, the tilt axis points along an intermediate in-plane direction.[29]

The structural properties in this section were obtained with XRD, while data from ND are presented in Sec. III C 1. In Fig. 3(a) we show, for all x, the temperature dependence of the orthorhombic strain $s = 2(b_o - a_o)/(a_o + b_o)$, from which we have extracted the HTT↔LTO transition temperature, T_{HT}, as a function of doping. The maximum strain s the lattice reaches at low temperatures is directly, although nonlinearly, related to T_{HT}.[30] Both quantities show a monotonic decrease with increasing x, as shown in the inset to Fig. 3(a) and in Fig. 3(b). In particular, we observe that T_{HT} decreases at a rate dT_{HT}/dx of ∼23.1 K/0.01 Ba [solid line in Fig. 3(b)], which is very similar to published polycrystal data.[6,42,46] For stoichiometric oxygen content,[56] the difference between a crystal's T_{HT} value and this line can be used to estimate the deviation of its actual Ba concentration x' from the nominal x. Overall the data in Fig. 3(b) show that x is a fairly good representation of x'. Nevertheless, in the discussion in Sec. IV we will show that small discrepancies between our results and data in the literature can be reconciled in terms of x'.

The second transition, at T_{LT}, from LTO to either LTT or LTLO, causes a sudden drop of the orthorhombic strain at low temperatures, as one can see in Fig. 3(a). In particular, for $x = 0.115$, 0.125, and 0.135, we observe discontinuous LTO↔LTT transitions. The crystals with $x = 0.11$ and 0.095 show discontinuous LTO↔LTLO transitions with very weak strain remaining below T_{LT}; the strain continues to decrease at low temperatures and, for $x = 0.11$, eventually becomes zero. The crystal with $x = 0.155$ shows a discontinuous transition that results in a mixed LTLO-LTT phase, as is discussed in more detail in Sec. III D 1. (That crystal also consisted of several domains, but we were able to isolate the diffracted signal from a single-domain region.)

To examine the low-temperature transition in more detail, we have followed the temperature dependence of the (1,0,0) superstructure reflection, which is allowed in the LTT and LTLO phases, but not in the LTO phase. In Fig. 3(c) we show integrated intensities $I_{(100)}$ normalized with the (2,0,0) Bragg reflection as previously explained. As x increases, one can see that $I_{(100)}$ drops while T_{LT} grows. This behavior indicates that local structural parameters are involved in the mechanism

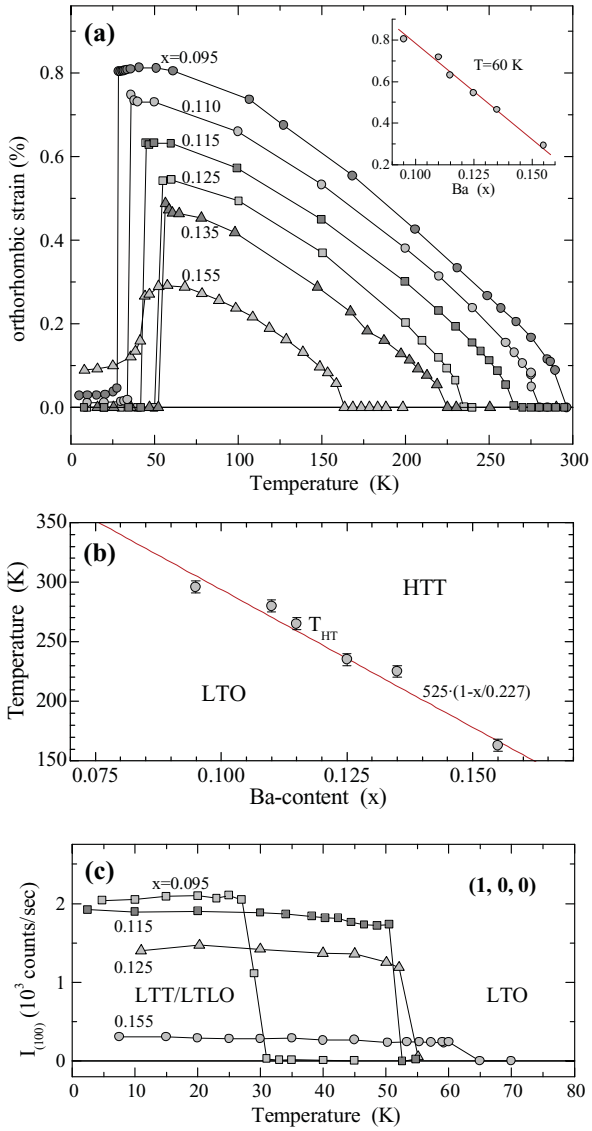

FIG. 3. (Color online) Structural properties of $La_{2-x}Ba_xCuO_4$ from XRD. (a) Orthorhombic strain s vs temperature as a function of Ba doping. s was determined from transverse scans through the (2,0,0)/(0,2,0) Bragg reflections that are simultaneously present owing to twin domains; see Fig. 2(e). For $x = 0.155$ the LTO↔LTLO transition of the majority phase is shown, although a significant volume fraction of 20% turns LTT at T_{LT}; see Fig. 14. Inset: s vs x at 60 K. The solid line is a guide to the eye. (b) Temperature of the HTT↔LTO transition vs doping. The solid line describes $T_{HT}(x)$ using $T_{HT}(0) \times (1 - x/x_c)$. $T_{HT}(0)$ and x_c were chosen such that at $x = 0$ the line intercepts at 525 K for La_2CuO_4 and goes through 235 K at $x = 0.125$, which is the most accurately known T_{HT} for Ba-doped compounds. (c) Integrated intensity from k scans through the (1,0,0) superstructure peak. For (a) and (c) error bars are within symbol size.

that drives the transition, as will be discussed further in Sec. IV.

At this point we mention that the low-temperature transition is also visible in the static magnetic susceptibility for dopings $x \leqslant 0.135$, and we find good agreement with the diffraction data for T_{LT}; see Fig. 10 and Ref. 61.

B. Charge stripe order

The CO, studied with XRD, leads to weak reflections with ordering wave vectors $\mathbf{Q}_{CO} = (2\delta,0,0.5)$ and $(0,2\delta,0.5)$, where δ increases with hole concentration; see Fig. 2(d).[62,63] While earlier studies have focused mainly on reflections at low ℓ, such as $(2 \pm 2\delta,0,0.5)$,[13,14,64] it was realized in more recent works that strong CO reflections can also be found at higher ℓ such as $\ell = 5.5$ and 8.5.[20,65,66] A conclusive analysis presented by Kim *et al.* in Ref. 20 shows that high-ℓ CO reflections appear, because CO not only causes displacements parallel to the CuO_2 planes but also in the perpendicular direction.

In Fig. 4 we show h and k scans through the $(2 + 2\delta,0,5.5)$ CO peak for different x at base temperature. Except for the k scan for $x = 0.115$, all scans were performed on samples with optimized thickness, so that peak intensities can be compared quantitatively as explained in Sec. II. The CO-peak positions were determined relative to the (2,0,6) Bragg reflection. Moreover, all scans were performed with identical scattering geometry, for which we kept the $[0,1,0]_t$ direction in the scattering plane. This guarantees the same relative orientation in k space of the CO peak and the resolution ellipsoid, which has been determined at the (2,0,6) Bragg peak; in Fig. 4, the resolution-limited peak shapes along h and k are indicated for $x = 0.125$.

As one can see in Fig. 4, the peak intensity is maximum at $x = 1/8$ and falls off rapidly for $x \neq 1/8$. To our surprise, we still find weak CO peaks for dopings as low as $x = 0.095$ and as high as $x = 0.155$. Furthermore, the width of the CO peak broadens for $x \neq 1/8$, which is particularly clear for the transverse k scans where the resolution is quite high, because it is determined by the mosaic of the LTT phase with typical values between 0.01° and 0.03°. In contrast, the resolution for the h scans is relatively poor and determined by the energy resolution $\Delta E/E$ of ~0.5% as well as the coarse instrumental resolution perpendicular to the scattering plane. Therefore, we have extracted all correlation lengths for the CO from transverse scans, as will be discussed in Sec. IV A.

The incommensurability 2δ extracted from the peak position in the h scans in Fig. 4 shifts monotonically from 0.205 for $x = 0.095$ to 0.245 for $x = 0.155$. The empirical relationship[63] $\delta \approx x$ for $x \leqslant 1/8$ would predict $2\delta = 0.25$ at $x = 0.125$, but the experimental value clearly stays below, as has been noticed by other groups, as well.[49]

In Fig. 5 we compare the temperature dependence of the CO and the (1,0,0) peak intensities for the different dopings. This time we show normalized integrated intensities since not all data sets do correspond to identical reflections, scattering geometry, or sample thickness. One important finding is that for $x \leqslant 0.135$ the onset of CO always coincides with the LTO→LTT/LTLO transition, i.e., $T_{CO} = T_{LT}$. Only for $x = 0.155$ does T_{CO} drop below T_{LT}. The temperature dependence of the CO and (1,0,0) peak intensities evolve differently. Independent of x, the (1,0,0) peak shows very sharp transitions, and is nearly constant below T_{LT}. This is indicative of the transition's first-order nature and shows that in the LTT phase the tilt angle Φ, and in the LTLO phase both Φ and the tilt direction, barely change at low temperatures.[6,29] In the case of the CO peak, we see an evolution from a sharp transition at $x = 0.095$ to one at $x = 0.135$, where CO fades away on

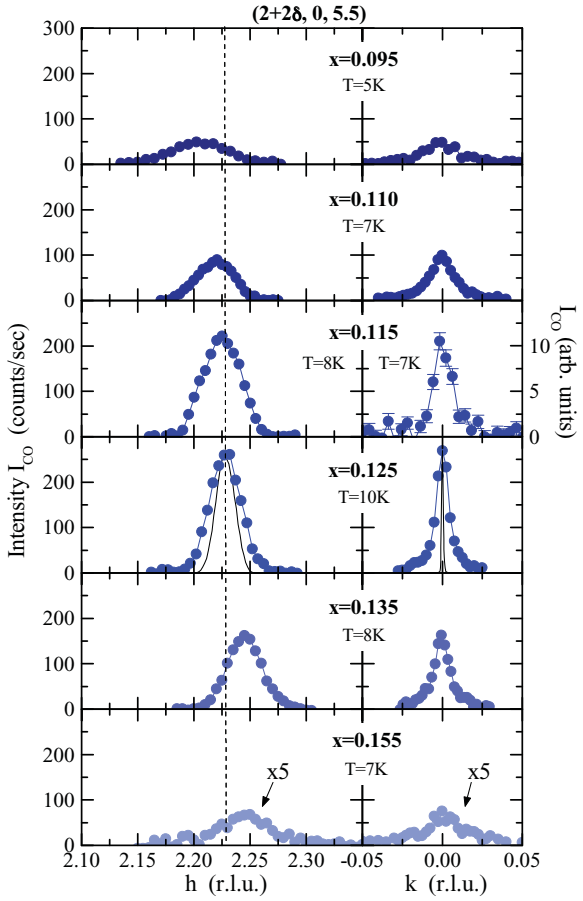

FIG. 4. (Color online) In-plane CO correlations. h scans (left) and k scans (right) through the CO peak at $(2+2\delta,0,5.5)$ for different dopings after subtraction of a linear background. Except for the k scan for $x = 0.115$, all intensities are normalized to the integrated intensity of the (2,0,6) Bragg reflection, as explained in Sec. II, and are directly comparable. Error bars are not shown if within symbol size. The data for $x = 0.155$ has been multiplied by a factor of 5. The dashed line marks the CO-peak position for $x = 0.125$ and emphasizes its shift with doping. All scans were collected in the same scattering geometry. The resolution functions along h and k were measured at the (2,0,6) Bragg reflection and are indicated by black solid lines for $x = 0.125$.

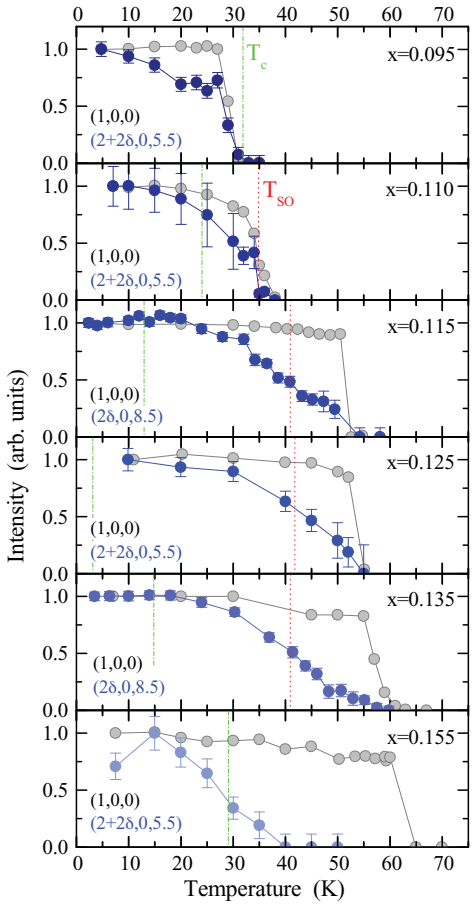

FIG. 5. (Color online) Integrated intensity vs temperature and doping from k scans through the (1,0,0) peak and h scans through the CO peak. Note that the data in this figure was not measured for all dopings in the same scattering geometry and in the case of the CO peak not always at the same (h,k,l) position. Therefore, presented intensities are normalized at low temperature. Error bars for the (1,0,0) intensity are within symbol size. The green dashed-dotted lines indicate the onset of bulk SC at T_c and the red dotted lines the onset of SO at T_{SO}.

warming, until finally at $x = 0.155$ we find $T_{CO} < T_{LT}$. For $x = 0.095$ in particular, the data suggest that CO could persist at higher temperatures if it were not cut off by the structural transition.

1. Charge stripe stacking order

An important question concerns the doping dependence of the stripe correlations perpendicular to the CuO_2 planes. For $x = 1/8$, the stacking arrangement in $La_{2-x}Ba_xCuO_4$ and $La_{1.6-x}Nd_{0.4}Sr_xCuO_4$ is well known. Stripes run parallel to the Cu-O bonds but in orthogonal directions in adjacent planes. Thus, only in every other layer do stripes run parallel, but in addition they are shifted by half the charge period, which results in a body-centered type of stacking, with a repeat of four planes (two unit cells).[12,14,17,20] Therefore, CO peaks occur at half integer ℓ positions.

To test the robustness of this stacking pattern as a function of hole concentration, we performed the ℓ scans shown in Fig. 6. Similar to Fig. 4, the data show absolute intensities obtained in identical scattering geometry. It is obvious that, in spite of the dramatic variation of the intensity, all scans show the same modulation in ℓ. This clearly demonstrates that the stacking order type is the same in the studied range $0.095 \leqslant x \leqslant 0.135$, and rules out a dramatic change of the correlation length perpendicular to the planes. Note that for $x = 0.155$ the intensity was too weak to identify the ℓ dependence.

Another question concerns the way the CO melts as the temperature approaches T_{CO}. There is evidence for $x = 1/8$, as well as for isostructural nickelates such as $Nd_{1.67}Sr_{0.33}NiO_4$, that the stacking order melts well before the in-plane order disappears at T_{CO}.[20,67] To check if our crystals show this effect, we performed scans through the $(2\delta,0,8.5)$ CO peak along h and ℓ for $x = 0.115$, 0.125, and 0.135; see Fig. 7. The data in Figs. 7(a) and 7(b) for $x = 0.125$ clearly show that the peak in ℓ remains well defined until it disappears simultaneously with the peak in h. In Figs. 7(c)–7(e) we show the integrated intensities of the h and ℓ scans for three dopings, normalized at the base temperature of ∼3 K. One can see that in all cases

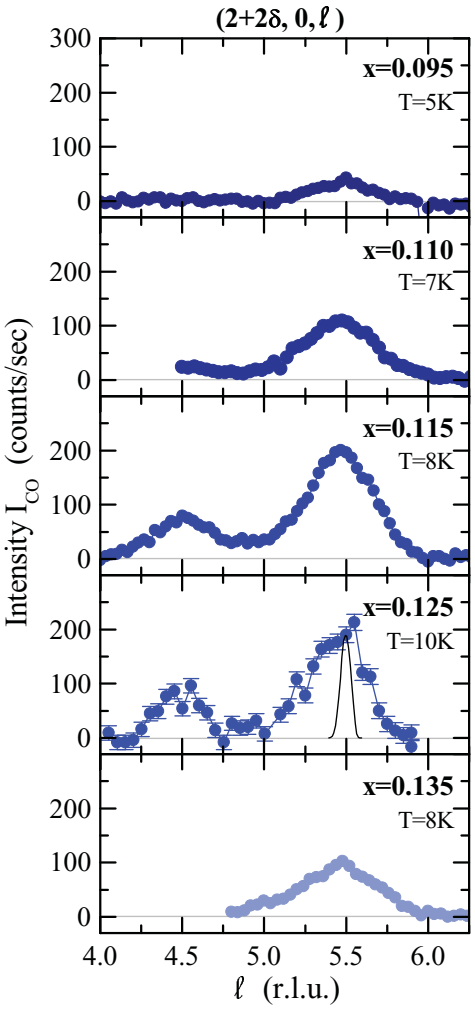

FIG. 6. (Color online) Interlayer CO correlations. ℓ scans along $\mathbf{Q} = (2 + 2\delta,0,\ell)$ at base temperature for different dopings after background subtraction. Intensities are normalized to the integrated intensity of the (2,0,6) Bragg reflection, as explained in Sec. II, and are directly comparable. The data for $x = 0.125$ has been taken from Ref. 34 and was measured in a pressure cell, which explains the low counting statistic. The data has been corrected for the absorption of the pressure cell. All scans were collected in the same scattering geometry. Error bars are not shown if within symbol size. The resolution function was measured at the (2,0,6) Bragg reflection and is indicated by the black solid line for $x = 0.125$. Because of a significant doping and temperature dependence of the background, there is no unique way to subtract it. In most cases the background was either measured along the same $\mathbf{Q}$ at $T \gtrsim T_{LT}$, or along $\mathbf{Q} = (2 + 2\delta, 0.03, \ell)$ at base temperature.

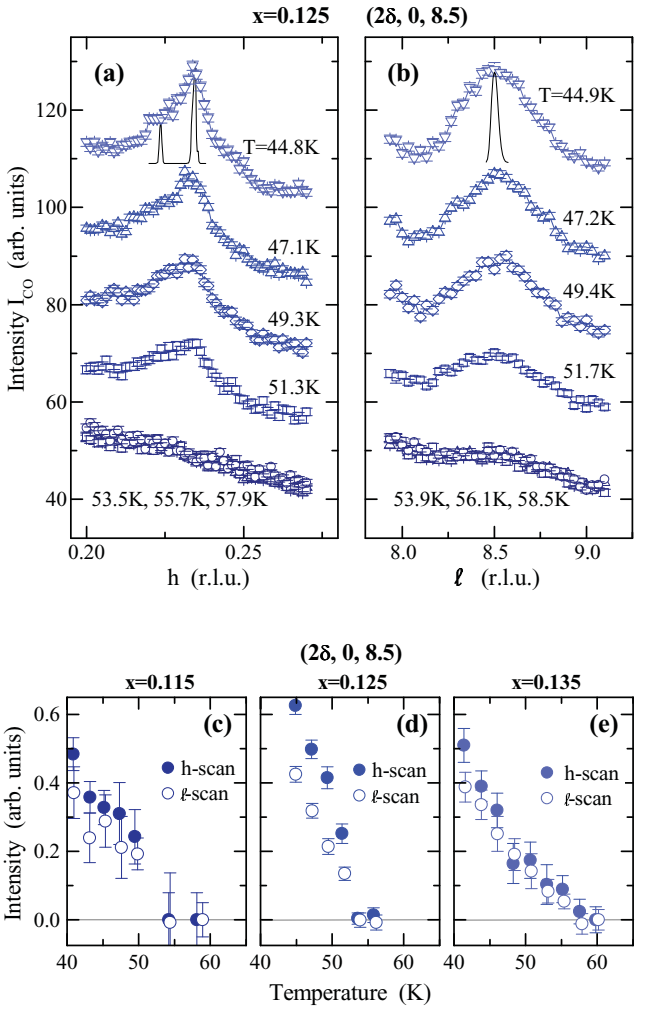

FIG. 7. (Color online) Melting of the CO. (a) h scans and (b) ℓ scans through the (2δ,0,8.5) CO peak for $x = 0.125$ at different temperatures. The remaining profile in the ℓ scans for $T > T_{CO}$ originates from diffuse scattering around (0,0,8). Curves for $T < T_{CO}$ are shifted for clarity. The black solid lines indicate the resolution function measured at the (0,0,8) Bragg reflection. The mosaic of the (0,0,8) reflection reveals the presence of two domains contributing to the CO peak. The orientation matrix was determined based on the peak positions of the larger domain. (c)–(e) Integrated intensities from corresponding h and ℓ scans for $x = 0.115$, 0.125, and 0.135. The data in (c)–(e) was normalized at a base temperature of ~3 K where additional scans were performed.

the extracted intensities for h and ℓ disappear simultaneously. Thus, we conclude that the stacking order persists up to T_{CO}, and that the CO melts isotropically.

We mention that the measurements in Fig. 7 were performed with the $(h,0,\ell)$ zone parallel to the scattering plane, where the high transverse resolution largely applies to the h scans through the (2δ,0,8.5) peak, and the lower longitudinal resolution largely to the ℓ scans, as indicated by the scans through the (0,0,8) Bragg reflection. Thus, h scans in this geometry are better suited to determine the in-plane CO correlation length perpendicular to the stripe direction than the h scans through $(2 + 2\delta,0,5.5)$ in Fig. 4. Corresponding data at base temperature will be discussed in Fig. 16 of Sec. IV A, together with selected k scans from Fig. 4 suited to extract the CO correlation length parallel to the stripe direction.

C. Spin stripe order

1. Neutron diffraction

The SO was studied by means of neutron diffraction and static magnetization measurements. Neutron diffraction allows one to directly probe the incommensurate spin structure of the SO and thus provides crucial complementary information

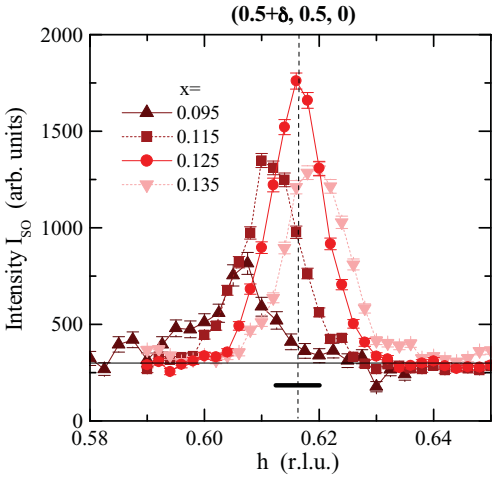

FIG. 8. (Color online) In-plane SO correlations. h scans through the SO peak at $(0.5+\delta,0.5,0)$ for different dopings. The horizontal bar at the bottom indicates the instrumental resolution full width at half maximum (FWHM) of 0.0078 r.l.u. The intensities have been normalized to the crystal volume in the neutron beam and for $x \geqslant 0.115$ are directly comparable; see text and Sec. II.

to the XRD data on the incommensurate CO. The magnetic ordering wave vectors are $\mathbf{Q}_{SO} = (0.5-\delta,0.5,0)$ and $(0.5,0.5-\delta,0)$, i.e., they are displaced by δ from the position of the magnetic Bragg peak in the AF parent compound La_2CuO_4, as indicated in Fig. 2(d). In Fig. 8 we show h scans through the $(0.5+\delta,0.5,0)$ SO peak for the different dopings. The data for $x \geqslant 0.115$ was taken at SPINS with an identical configuration and is normalized to the crystal volume in the beam, thus allowing a direct comparison of the intensities. One can see that the SO peak is maximum for $x = 1/8$, just as for the CO peak. The data for $x = 0.095$ were taken with the HB-1 spectrometer; they show a SO peak that is definitely much weaker, although the available data is insufficient to draw a precise quantitative comparison to the other dopings. No SO peak was detected for $x = 0.155$, which could be because stripe order has become very weak. On the other hand, this crystal is a good bulk superconductor with $T_c = 29$ K, so it could be that there is a spin gap below T_c in place of a SO peak.[68] As one can see in Fig. 8, the SO peak shifts to higher h with increasing x, reflecting a similar increase of δ as for the CO peak; details will be discussed in Sec. IV.

Next, in Fig. 9 we compare the temperature dependence of the peak intensity of the (1,0,0) peak and the SO peak as measured with ND. The first thing to note is the good agreement of the (1,0,0) data in Fig. 9(a) with corresponding XRD data in Fig. 5 regarding $T_{LT}(x)$ and the sharpness of the LTO↔LTT/LTLO transitions, considering the experimental errors resulting from the use of different instruments, and the fact that the neutron beam averages over a sample volume that is three orders of magnitude larger than for XRD. This indicates a high homogeneity of the crystals' stoichiometry and quality.

Figure 9(b) shows the SO-peak intensity as a function of temperature. One can see that for $x \geqslant 0.115$, intensity sets in at a temperature below T_{LT}. The gap to T_{LT} is particularly wide for $x = 0.135$, but also clearly visible for $x = 0.115$ and

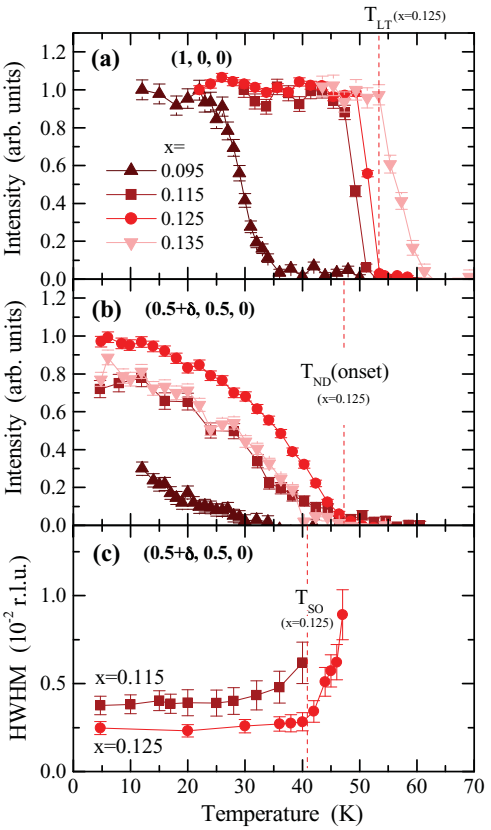

FIG. 9. (Color online) Peak intensity vs temperature and doping of (a) the (1,0,0) superstructure peak normalized at low temperature and (b) the $(0.5+\delta,0.5,0)$ SO peak normalized to the crystal volume in the neutron beam. The data in (b) are directly comparable only for $x \geqslant 0.115$; see text and Sec. II. (c) Resolution corrected half width at half maximum (HWHM) of h scans vs temperature for $x = 0.115$ and $x = 0.125$. The dashed lines in (a)–(c) indicate the onset temperatures for $x = 0.125$ of the LTO↔LTT transition, the SO peak intensity, and the peak broadening. Data for $x = 0.125$ previously presented in Ref. 36.

0.125. For $x = 0.095$, the onset is ~30 K, but the low statistics of the weak signal prevents a precise correlation with the other transitions.

It is known from, e.g., muon spin rotation (μSR) measurements[69,70] that truly static SO sets in below the onset temperature seen by neutron diffraction. The difference is owing to the coarser energy resolution of neutron diffraction, which can sample critical fluctuations at $T > T_{SO}$. In Ref. 36 we have argued, for the case of $x = 0.125$, that T_{SO} coincides with the temperature above which the SO peak starts to broaden; see corresponding data for two dopings in Fig. 9(c). Furthermore, we have shown in Refs. 35 and 51 for $x = 0.125$ that T_{SO} is also marked by a weak ferromagnetic-type transition in the static magnetic susceptibility for magnetic fields $H \parallel ab$, which we discuss next.[71]

2. *Static magnetic susceptibility*

In Fig. 10 we compare the static susceptibility χ for dopings $0.095 \leqslant x \leqslant 0.155$. The core diamagnetism and the Van Vleck susceptibility of the Cu^{2+} ions have not been subtracted.[51] The top panels of Fig. 10 are for $H \parallel c$, and the

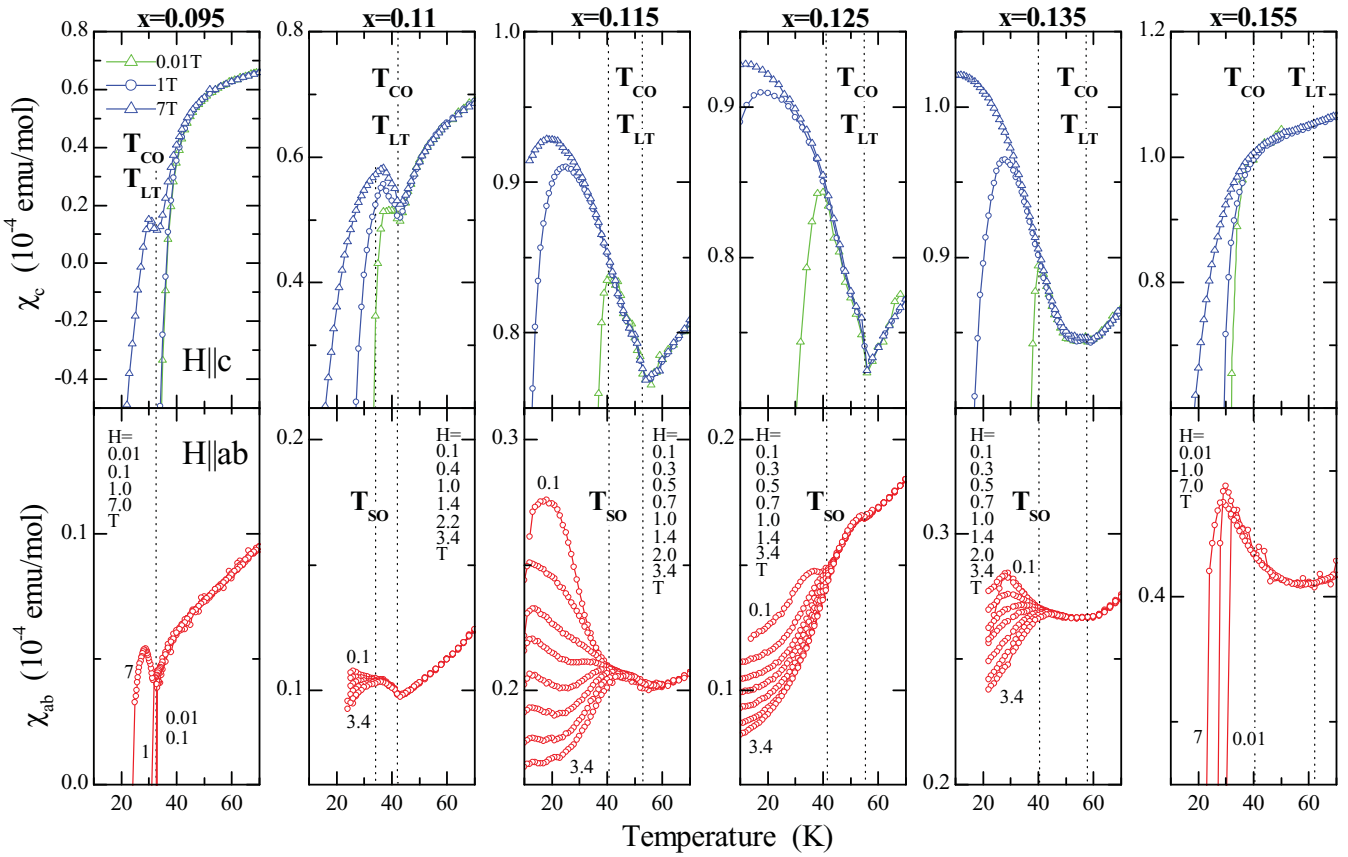

FIG. 10. (Color online) Field-cooled static susceptibility $\chi = M/H$ of $La_{2-x}Ba_xCuO_4$ vs temperature for different dopings and magnetic fields applied parallel to the c axis (top) and parallel to the ab plane (bottom). Similar to Ref. 51, small deviations between curves for same x but different fields, owing to experimental error ($\pm 0.007 \times 10^{-4}$ emu/mol), were corrected by shifts in χ, so that curves match for $T > T_{LT}$ where no field dependence was observed. CO leads to anomalies most pronounced for $H \parallel c$. SO is identified by means of a weak ferromagnetic type transition for $H \parallel ab$. One can see that T_{SO} also coincides with the onset of weak diamagnetism from superconducting correlations for $H \parallel c$. Furthermore, for $x \leqslant 0.135$ T_{CO} coincides with T_{LT}. For $x = 0.155$ no anomalies are observed and T_{CO} and T_{LT} are from XRD. For $x = 0.095$ only one transition at $T_{CO} = T_{LT}$ is observed. We have limited the data for $H \parallel ab$ to fields below the spin-flop transition (Ref. 51), which will be the focus of a future publication.

bottom panels for $H \parallel ab$. The dashed lines mark the onset of SO and CO as well as the LTO↔LTT/LTLO transition. One can see that the CO transition leads to anomalies most pronounced for $H \parallel c$. Moreover, the data for $H \parallel c$ display the suppression of diamagnetic contributions to the normal state susceptibility from SC, which leads to an *increase* of χ_c with field. In contrast, the data for $H \parallel ab$ display the weak ferromagnetic-type behavior, which is visible for $0.11 \leqslant x \leqslant 0.135$ and characterized by a *decrease* of χ_{ab} with field for $T < T_{SO}$. In the case of $x = 0.095$ and $x = 0.155$ and $H \parallel ab$, the static susceptibility reveals no information on SO, simply because the onset of bulk SC has shifted to higher temperatures and obscures any signature of the normal state weak ferromagnetism.

It is remarkable to see in Fig. 10 that, for those x displaying the weak ferromagnetic-type moment for $H \parallel ab$, T_{SO} coincides with the temperature T_c^* of first appearance of superconductivity for $H \parallel c$ in the limit of small magnetic fields; see dashed lines denoting T_{SO}. Note that in Fig. 10 we are looking at an extremely fine scale. For comparison, 1×10^{-4} emu/mol equals only 0.0023% of the full Meissner response. In Refs. 35 and 36 we have discussed the idea that in $La_{1.875}Ba_{0.125}CuO_4$ this weak diamagnetism in the LTT phase emerges from two-dimensional (2D) superconducting fluctuations below T_c^*, rather than three-dimensional (3D) bulk superconductivity, which sets in at a lower temperature T_c and will be discussed in Sec. III D. Here we have shown that $T_{SO} = T_c^*$ in a broader range of doping around $x = 1/8$.

Note that the scope of the present work is to highlight the fingerprints in χ_c and χ_{ab} that have been essential to construct the stripe phase diagram in Fig. 1. A detailed analysis of the bare spin susceptibility, as performed in Ref. 51 for $La_{1.875}Ba_{0.125}CuO_4$, will be presented for all x in a forthcoming publication. We also mention that the origin of the small moment is not yet understood. Angle-dependent measurements have shown that it is confined to the CuO_2 planes. The moment saturates at a field of ~1 T, which is much lower than the in-plane spin-flop field of ~6 T identified in Ref. 51 for $x = 0.125$. Although the field dependence of the moment resembles that of a ferromagnet, its hysteresis or remanent moment are too small to be resolved. The reason for that is the small size of the moment, which is approximately two orders of magnitude smaller ($\sim 10^{-5} \mu_B$/Cu) than the

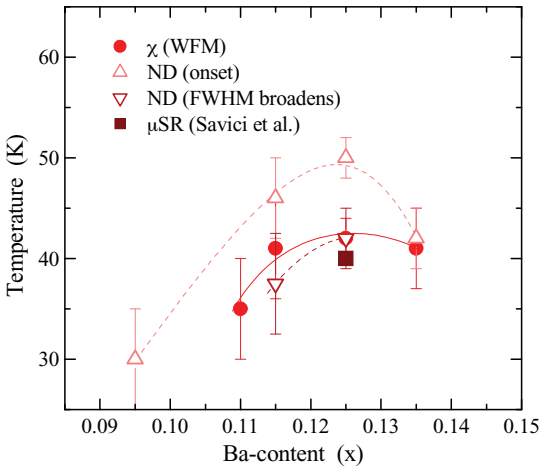

FIG. 11. (Color online) Critical temperatures of the SO transition in $La_{2-x}Ba_xCuO_4$ single crystals. (△) Onset of SO peak intensity and (▽) saturation temperature of SO-peak width as measured with ND, (●) onset of weak ferromagnetic (WFM) type signal for $H \parallel ab$ in static magnetic susceptibility, which we associate with T_{SO}. (■) T_{SO} as measured with μSR; taken from Ref. 69.

well-characterized spin canting perpendicular to the planes in pure La_2CuO_4, caused by Dzyaloshinsky-Moriya superexchange ($\sim 10^{-3}\mu_B$/Cu). As discussed previously,[72] spin canting in the stripe phase, if present, would be largely invisible to the bulk susceptibility owing to the antiphase spin correlations across a charge stripe.

3. *Comparison of critical temperatures*

In Fig. 11 we compare the various critical temperatures of the SO phase, extracted by ND and χ measurements as well as by μSR in Ref. 69. There is good agreement for T_{SO} from χ and μSR as well as from the SO-peak broadening in ND, whereas the onset temperatures of finite SO-peak intensity are higher. For the phase diagram in Fig. 1 we decided to show T_{SO} from χ, because this is the most complete and precise set of values. Only for $x = 0.095$ did we take the onset temperature from ND, knowing that truly static SO most likely occurs at a lower temperature. For $0.11 \leqslant x \leqslant 0.135$, where we are more confident of the determination, one can see from Fig. 1 that T_{SO} is always lower than T_{CO}.

Returning to Fig. 10, we reconsider the finding that the anomalies in χ at T_{LT} are particularly pronounced for $H \parallel c$ and $x \leqslant 0.125$; see the dashed lines. For these dopings we know that $T_{CO} = T_{LT}$. In contrast, the anomaly is quite small in the case of $x = 0.135$, where χ_c starts to increase significantly only for $T < 50$ K. This is consistent with the sample's CO in Fig. 5, which becomes already weak at $T \sim 50$ K before it eventually disappears at T_{CO}. Because the structural changes at T_{LT} for $x = 0.135$ and $x = 0.125$ are not so dramatically different, this tells us that the anomaly in χ_c must be sensitive to the CO. Finally, for $x = 0.155$ with its extremely weak CO, there is no anomaly at either T_{LT} or T_{CO}.

D. Superconductivity

The bulk SC phase was analyzed by magnetic susceptibility measurements. In Fig. 12 we show a selection of normalized

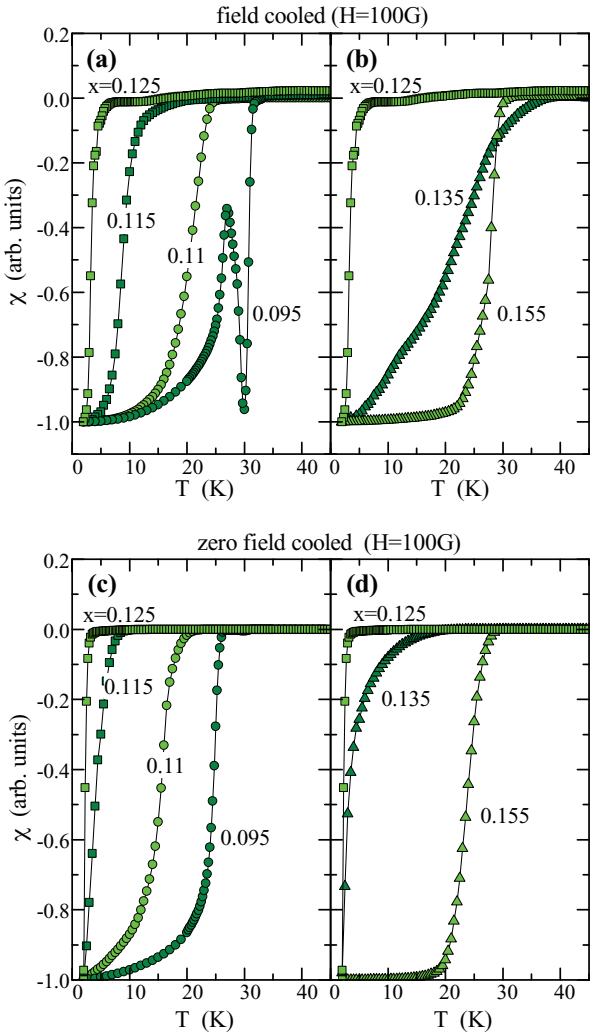

FIG. 12. (Color online) Superconductivity in $La_{2-x}Ba_xCuO_4$. Normalized FC (top) and ZFC (bottom) susceptibility vs temperature for a magnetic field of $H = 100$ G applied parallel to the c axis. Data in (a) and (c) are for $x \leqslant 1/8$ and in (b) and (d) for $x \geqslant 1/8$.

field-cooled (FC) and zero-field-cooled (ZFC) measurements for a magnetic field of $H = 100$ G (0.01 T) applied parallel to the c axis. Similar data sets for 2 and 20 G reveal no additional information. The data are normalized at 2 K; see the explanation in Ref. 73. The left-hand panels in Fig. 12 show how the bulk T_c decreases for $x \geqslant 0.095$, reaching a minimum at 1/8 doping, while the right-hand panels show how T_c increases again for $x > 1/8$. The bulk SC transition temperatures shown in Fig. 1 were each determined from the intercept of the tangent to the steepest part of the FC curve with $\chi = 0$, for all except $x = 0.135$. The latter crystal has a very broad transition, as one can see best in Fig. 12(d), which may originate from a very steep phase boundary in that region, i.e., large dT_c/dx, or sample inhomogeneity. In addition, the crystal has a very small Meissner signal, so that the normalization overemphasizes its diamagnetic signal with respect to the other FC curves in Fig. 12(b). Therefore, we decided to identify the T_c for $x = 0.135$ with the onset temperature in the ZFC curve.

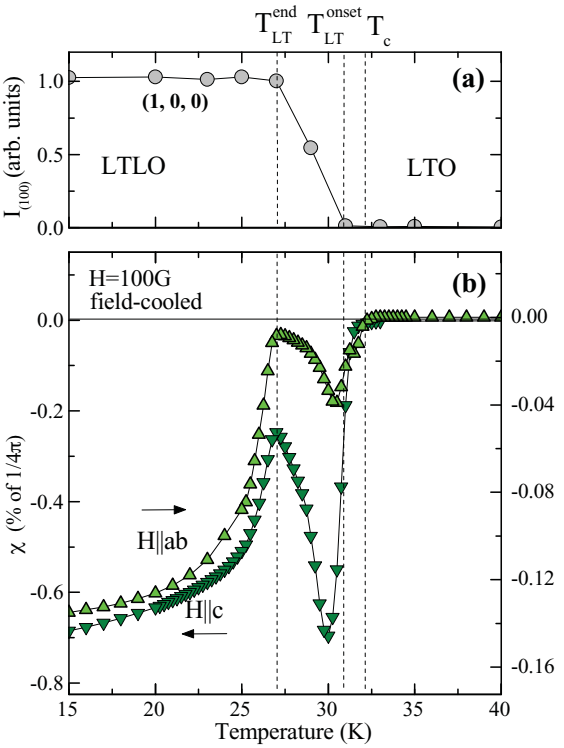

FIG. 13. (Color online) Superconductivity and stripe order in $La_{1.905}Ba_{0.095}CuO_4$. (a) Integrated intensity of the (1,0,0) superstructure reflection. (b) FC signal for $H = 100$ G applied parallel to the c axis and the ab plane. T_c indicates the onset of bulk SC in the LTO phase. T_{LT}^{onset} and T_{LT}^{end} denote the onset and the completion of the LTO→LTLO transition, respectively.

1. Special cases x = 0.095 and x = 0.155

To properly judge the bulk SC properties of the crystals with $x = 0.095$ and $x = 0.155$, we emphasize some unique features not observed for the other samples. The crystal with $x = 0.095$ is interesting, because it is the only crystal where the LTO↔LTLO transition occurs just below the SC transition. As one can see in Fig. 13, after the initial onset of bulk SC in the LTO phase at $T_c = 32$ K, SC collapses below 30 K when both the LTO→LTLO and the CO transition occur. Once the transformation is complete, bulk SC reappears. The fact that even at low T the FC signal stays below 1% of the full Meissner response is owing to strong flux pinning in large single crystals.[73]

The crystal with $x = 0.155$ is special because it is the only one that does not show a clean structural transition to single-phase LTT or LTLO. Instead, the LTO phase transforms into a phase mixture of LTT and LTLO with a volume ratio of 1:4; see Fig. 14. Between T_{LT} and base temperature, the orthorhombic strain of the LTLO phase continues to decrease monotonically; see also Fig. 3. It remains unclear whether CO exists only in the LTT phase or also in the LTLO phase. In a study on $La_{1.875}Ba_{0.125-y}Sr_yCuO_4$, static CO was observed in crystals with LTLO phase with significantly larger remanent strain,[74] however, the situation could be different for $x \neq 0.125$. For these reasons the contributions of the LTT and LTLO phase fractions to both bulk SC below T_c, and CO below T_{CO} remain unquantifiable for the $x = 0.155$ crystal.

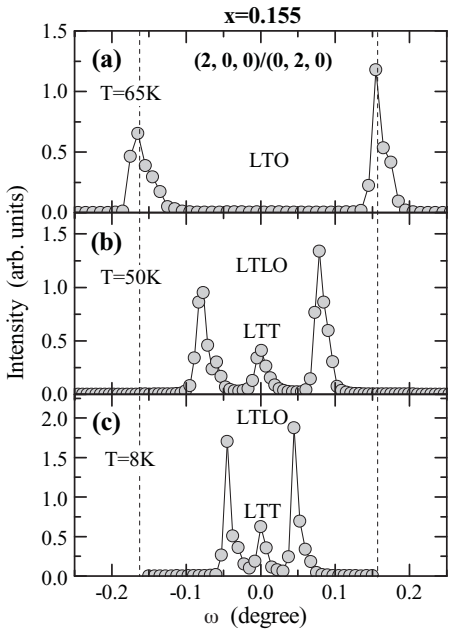

FIG. 14. Low-temperature phase transition in $La_{1.845}Ba_{0.155}CuO_4$. ω scans through the (2,0,0)/(0,2,0) Bragg reflections that are simultaneously present owing to twin domains; see Fig. 2(e). (a) In the LTO phase just above the phase transition, (b) in the mixed LTLO and LTT phase below the transition, and (c) at base temperature. Error bars are within symbol size.

IV. DISCUSSION AND CONCLUSIONS

The successful growth of $La_{2-x}Ba_xCuO_4$ single crystals with Ba concentrations as high as $x = 0.155$ has given us the opportunity to study the stripe phase beyond the magic 1/8 anomaly and even up to optimal doping, a region that has so far only been accessible with polycrystalline materials.[2,6,11,28,75] The detection of CO in bulk SC crystals with x far below and far above $x = 1/8$ is certainly the most significant finding. The full picture, however, becomes clear only when considering the relationship between the various properties and transition temperatures.

A. Variation of parameters with nominal Ba content

A summary of important parameters versus Ba doping is given in Fig. 15. In Fig. 15(a) we compare T_{HT} with the octahedral tilt angle Φ of the average structure calculated from the orthorhombic strain just above T_{LT}. Besides the monotonic variation of T_{HT} and Φ, one can see that stripe order occurs for tilt angles ranging at least from 4.0° to 2.4°, with stripes being most stable at $x = 1/8$ where $\Phi = 3.3°$. For $La_{2-x-y}Nd_ySr_xCuO_4$ a critical tilt angle of 3.6° has been identified to mark a phase boundary between SC and non-SC in the LTT phase.[30] This boundary is not very sharp and there are no reports yet on how deep CO persists into the SC LTT region with $\Phi < 3.6°$. The existence of such a critical angle is reasonable, because the symmetry-breaking potential of the LTT phase should scale with Φ. However, in our recent high-pressure experiments on $La_{2-x}Ba_xCuO_4$ at $x = 1/8$ we have found that CO forms even for $\Phi = 0$, where the average structure has flat CuO_2 planes.[34] We believe that in

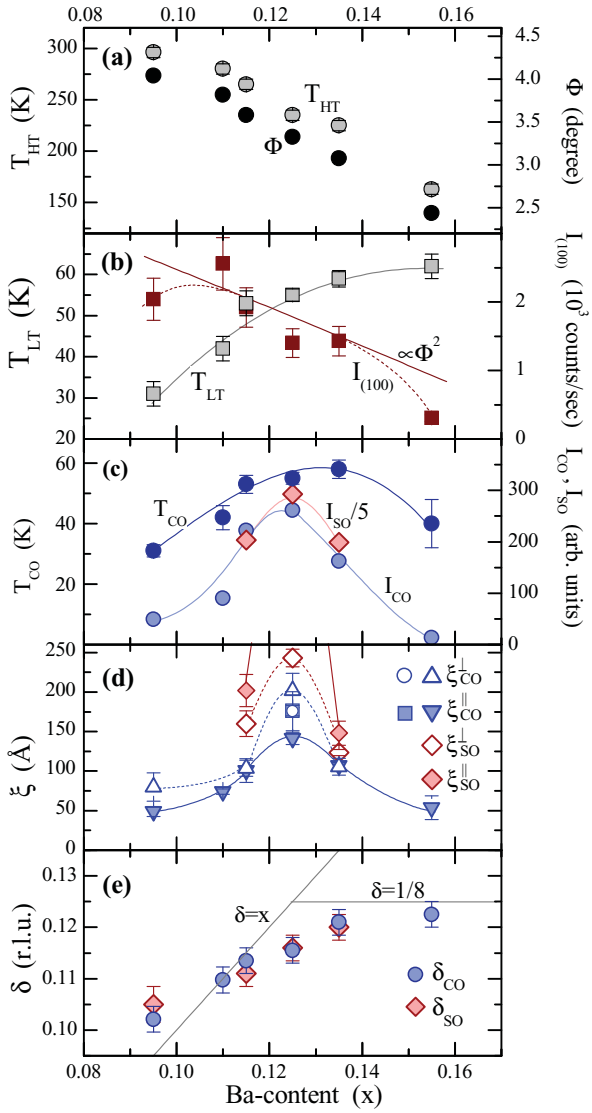

FIG. 15. (Color online) Crucial parameters of stripe phase and crystal structure in $La_{2-x}Ba_xCuO_4$ vs nominal Ba content. (a) HTT↔LTO transition temperature T_{HT} and octahedral tilt angle Φ at 60 K of average structure. Φ was calculated using $\Phi^2 = f(b_o - a_o)$ with $f = 380$ (deg)^2/Å for the tilt of the apical oxygen (Refs. 30 and 76). (b) LTO↔LTT/LTLO transition temperature T_{LT} and integrated intensity of the (1,0,0) peak at base temperature. The solid line through $I_{(100)}$ is a scaled fit to the square of the Φ data in (a). (c) Charge stripe order temperature T_{CO} as well as peak intensity of CO and SO-peaks. (d) In-plane correlation lengths ξ of CO and SO parallel (∥) and perpendicular (⊥) to the stripe direction at base temperature. At $x = 0.125$ there is an additional point for $\xi^{\parallel}_{SO}$ at ∼600 Å. (e) Incommensurability δ extracted with XRD from the CO-peaks and with ND from the SO-peaks. In the case of δ_{CO} we have averaged the values extracted from the h scans in Figs. 4 and 16. The solid lines $\delta = x$ and $\delta = 1/8$ describe the low and high x reference of the stripe model. Solid and dashed lines in (b), (c), and (d) are guides to the eye, except for the solid line for Φ^2 in (b). Error bars are not shown if within symbol size.

this latter case the interactions between dynamic short-range charge stripe correlations and local octahedral tilts trigger a spontaneous symmetry breaking by stripes. This mechanism may be particularly strong for commensurate $x = 1/8$ doping. It is possible that the strength of the coupling to local displacements also depends on the local variance[77,78] of the ionic radii at the lanthanum site; that is, the critical Φ of the average LTT structure may be smaller for compounds with a larger variance. In fact, $La_{1.875}Ba_{0.125}CuO_4$ has a larger variance than $La_{1.475}Nd_{0.4}Sr_{0.125}CuO_4$, which may explain our observation of CO for $x = 0.155$ with only $\Phi = 2.4°$.

Further signatures of the influence of local properties of Ba are evident from Fig. 15(b), where we focus on the LTO↔LTT/LTLO transition. First we discuss the saturated intensity of the (1,0,0) peak at low temperatures. For the crystals with pure LTT ground state the (1,0,0) intensity is experimentally observed to roughly scale with Φ^2, as is indicated by the solid line that was obtained from a fit to the square of the Φ data in Fig. 15(a). Φ decreases with increasing Ba content, and becomes zero in the HTT phase.[5] In the LTLO phase, the (1,0,0) intensity also decreases with increasing orthorhombic strain, which explains why for $x = 0.155$ the (1,0,0) intensity drops below the scaled Φ^2 curve. For all other crystals the strain at base temperature is either zero or negligible. Hence, the observed decrease of the (1,0,0) peak toward high doping can be naturally explained in terms of Φ for the average structure. On the other hand, we see that T_{LT} increases with Ba doping in spite of the decrease of Φ and T_{HT}, thus requiring a different explanation. Here, local distortions around an increasing number of Ba defects must be the driving force for the transition, as has been discussed in Refs. 77 and 78. Toward low doping, the LTT (or LTLO) phase and thus the (1,0,0) peak eventually have to disappear, because there are just not enough Ba defects to stabilize these phases. The relatively low T_{LT} and (1,0,0) intensity for $x = 0.095$ are evidence of this.

In Fig. 15(c) we compare T_{CO} with the peak intensities of the CO peak and the SO peak. (For T_{SO}, see Fig. 11.) The similarity in trends for the CO and SO phases is apparent. Both peak intensities show a maximum at $x = 1/8$ and drop off quickly for $x \neq 1/8$. In contrast, T_{CO} and T_{SO} describe broad domes, which do not necessarily peak symmetrically at $x \sim 1/8$. For example, T_{CO} coincides with T_{LT} and increases up to at least $x = 0.135$. In the case of T_{SO}, our data indeed suggest a weak maximum at $x = 1/8$. This is consistent with polycrystal data from μSR in Ref. 11, which show a clear peak at $x = 1/8$, although the T_{SO} values are ∼10 K lower than in our single crystals. With SO transition temperatures as high as 42 K, the crystals' T_{SO} are reminiscent of the highest T_c of $La_{2-x}Sr_xCuO_4$ reached under pressure when the CuO_2 planes become flat.[5]

In Fig. 15(d) we show the in-plane correlation lengths ξ for the CO and SO at base temperature. As mentioned earlier all ξ values for the CO were extracted from transverse scans, a selection of which is presented in Fig. 16. For the CO at $x = 1/8$ two additional points are shown that were obtained from transverse h and k scans through the close-by (2δ,0,8.5) and (0,2δ,8.5) reflections of a second piece of crystal; see the filled square and open circle in Fig. 15(d). In general, we find that ξ is maximum at $x = 1/8$, but CO and SO show a qualitative difference with respect to the correlations parallel (∥) and perpendicular (⊥) to the stripe direction. While ξ is relatively isotropic for CO ($\xi^{\parallel}_{CO} \sim \xi^{\perp}_{CO}$), in the case of SO we

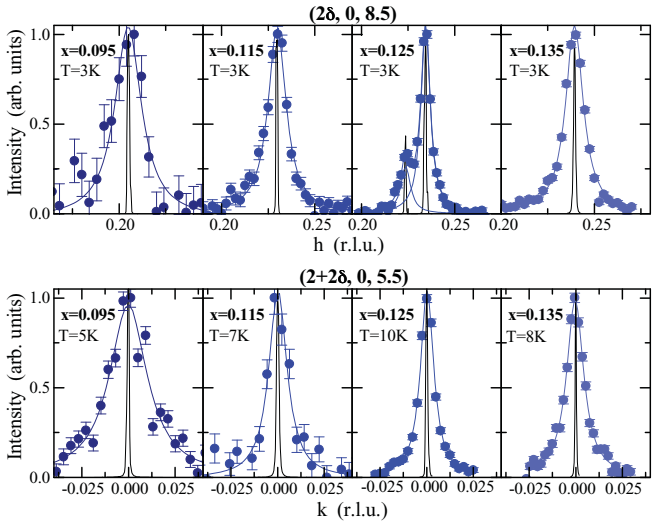

FIG. 16. (Color online) Comparison of CO-peak widths from transverse scans at base temperature for different dopings. Intensities are normalized and shown after subtraction of a linear background. Top: h scans through the $(2\delta,0,8.5)$ peak. Bottom: k scans through the $(2+2\delta,0,5.5)$ peak. The lines through the data are fitted Lorentzians. The resolution functions, indicated by black solid lines, were determined for each crystal and both scattering geometries by performing transverse scans through the (0,0,8) and (2,0,6) Bragg reflections, respectively. Note that in the $(h,0,\ell)$ plane (top) the crystal with $x = 0.125$ reveals the presence of two domains. The orientation matrix was determined based on the peak positions of the larger domain. Apart from the normalization, the k scans in the bottom panels are the same as in Fig. 4.

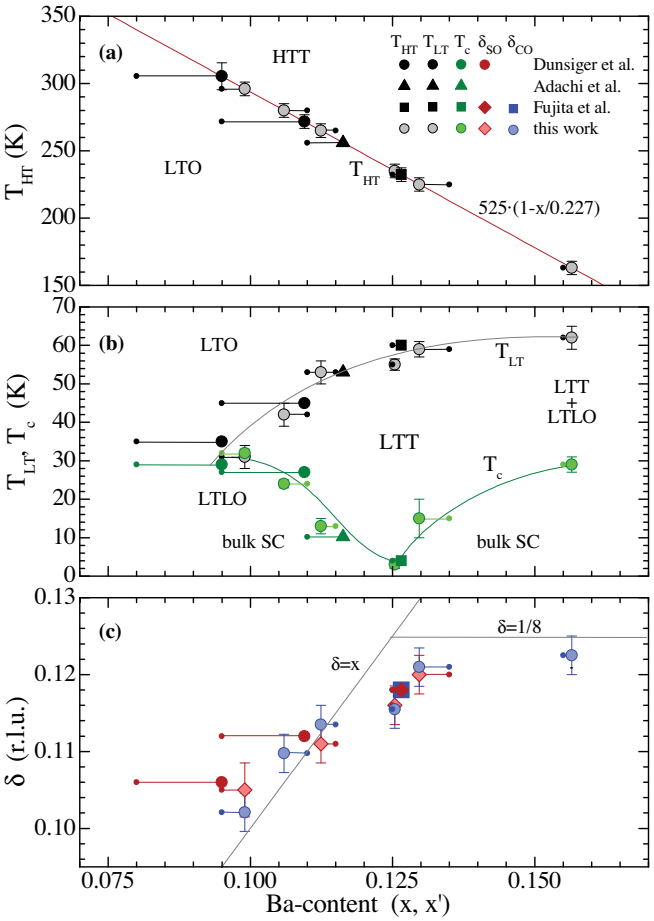

FIG. 17. (Color online) Comparison of selected parameters of $La_{2-x}Ba_xCuO_4$ from current work and literature plotted vs nominal (x) and calculated (x') Ba content. (a) Experimental data for T_{HT} and theoretical curve used to estimate actual Ba content. Small dots in (a)–(c) represent data plotted vs nominal Ba content, large symbols those vs calculated Ba content. (b) Structural and bulk SC transition temperatures T_{LT} and T_c. Solid lines are guides to the eye. (c) Incommensurability δ extracted with XRD from the CO peak and with ND from the SO peak. The solid lines describe the low and high x reference of the stripe model. (a)–(c) Where available, error bars are shown. The literature data were taken from Dunsiger *et al.* (Ref. 47), Adachi *et al.* (Ref. 42), and Fujita *et al.* (Ref. 18).

find the tendency $\xi_{SO}^{\parallel} > \xi_{SO}^{\perp}$ with a maximum anisotropy at $x = 1/8$. Here, $\xi_{SO}^{\parallel}$ reaches ~600 Å, as previously reported in Refs. 36 and 79. The observation that ξ_{SO} is generally larger than ξ_{CO} has been discussed in Refs. 14 and 31. In the case of ξ_{CO} qualitatively similar results, with respect to doping and anisotropy, have been reported in Ref. 49 for $La_{2-x}Ba_xCuO_4$ and $La_{1.6-x}Nd_{0.4}Sr_xCuO_4$.

Finally, we present the incommensurability δ in Fig. 15(e), for which we find good agreement between the values determined with XRD from the CO peak and with ND from the SO peak. In the phenomenological stripe model, one expects that δ follows the solid line $\delta = x$ for $x \leqslant 0.125$ and saturates, or increases less steeply, for $x > 0.125$.[62,63,74] Our data for δ match that line at $x \sim 0.11$, stay below for higher x, and seem to stay above toward lower x. Similar deviations have been reported in Ref. 47 for low x and in Ref. 49 for $x = 0.125$.

B. Estimated actual Ba content; comparison with literature

In this section, we will make the case that small discrepancies among different studies can be reconciled to a large extent by accounting for deviations of the actual Ba content x' from the nominal x value, where we assume that crystals grown in several bar of oxygen have a stoichiometric oxygen content; see Ref. 56. In this case the structural transition temperature T_{HT} is controlled by the Ba concentration. To use T_{HT} for calibrating x', we assume that it follows the linear dependence $T_{HT}(x) = T_{HT}(0) \times (1 - x/x_c)$, as shown in Fig. 17(a) [same as in Fig. 3(b)]. At $x = 0$ this curve assumes the experimental value $T_{HT} = 525$ K for La_2CuO_4 and it goes through 235 K at $x = 0.125$, which is the most accurately known value for Ba-doped compounds. In Fig. 17 we compare our data with single-crystal data from literature for both nominal x (small dots) and calculated x' (large symbols). In Figs. 17(b) and 17(c) one can recognize a significantly improved agreement between the various data sets for T_{LT}, T_c, and δ when plotted versus x'.

In particular, for $\delta(x')$ we find a much better agreement with the trend $\delta = x'$ for $x' < 1/8$ as shown in Fig. 17(c). Nevertheless, $\delta(x')$ still falls below $\delta = 1/8$ for $x' \geqslant 1/8$. This is in contrast to the observations in $La_{1.6-x}Nd_{0.4}Sr_xCuO_4$ with nominal $x = 0.12$ and 0.125, where the measured δ values are closer to the expected trend, and for $x = 0.15$ even exceed the 1/8 mark.[13,14,20,49,62] These quantitative differences need

further experimental clarification. In terms of the simple stripe picture, one may speculate that in $La_{2-x}Ba_xCuO_4$ with $x \gtrsim 1/8$ the hole concentration of the charge stripes is slightly higher than expected, or that not all doped holes participate in the CO, or at least less than in $La_{1.6-x}Nd_{0.4}Sr_xCuO_4$ with identical x.

C. Superconductivity and stripe order

A key question concerns the relationship between stripe order and SC. Are stripe correlations an essential and universal ingredient of SC in the cuprates, or just an interesting but not crucial feature? This multifaceted problem has attracted a lot of attention. Angle-resolved photoemission spectroscopy studies show that in the stripe ordered state $La_{2-x}Ba_xCuO_4$ develops a gapped Fermi surface similar to that in bulk SC $La_{2-x}Sr_xCuO_4$, with the antinodal gap energy $\Delta(x)$ of both groups of samples describing a dome with a maximum at $x \sim 1/8$.[44,55] This motivated the idea that static stripe order does not suppress SC pairing correlations per se, but prevents phase coherence.[35] In our recent work on $La_{1.875}Ba_{0.125}CuO_4$ we obtained further evidence for this picture. It seems that stripe order causes an electronic decoupling of the CuO_2 planes and destroys the 3D SC phase coherence, while some kind of 2D SC fluctuations survive.[35,36] Similar conclusions have been reached in recent theoretical work in which the specific stacking arrangement of stripes in $La_{2-x}Ba_xCuO_4$ was considered.[37,38]

If the CO and SO happened to compete with the amplitude of the SC order, then we might expect to see a decrease in CO and SO peak intensities at the onset of bulk SC. First we focus on the CO data in Fig. 5, where we have indicated T_c by vertical dashed-dotted lines. The best cases to examine are $x = 0.11$, 0.115, and 0.135, where T_c is well below T_{CO} but not too far below. As one can see, there is no significant change of the CO-peak intensity at T_c. Note that the crystal with $x = 0.155$ is not well suited for this test because of the low statistics of the CO data as well as the presence of the LTT/LTLO phase mixture.

In the case of SO, the best candidates are the crystals with $x = 0.115$ and 0.135. As can be seen in Fig. 9(b), no significant changes of SO at T_c are apparent. [This is in contrast to $Ba(Fe_{1-x}Co_x)_2As_2$, where the spin-density-wave order decreases with the onset of superconductivity.[80]] We mention that published work by other groups for $x < 1/8$ also bears no evidence for changes of SO or CO across T_c.[47,49] Another question is whether the onset of SO has any effect on the CO. It is thinkable that the onset of SO enhances the CO. However, in Ref. 36 we could show for $x = 1/8$ that neither the intensity nor the width of the CO peak are affected by the SO transition. The two other dopings where the current data allow conclusions are $x = 0.115$ and 0.135 with $T_{SO} \simeq 41$ K, but also in these cases no changes of the CO at T_{SO} are observed; see Fig. 5.

Overall, we find no evidence that CO and SO are affected by the onset of bulk 3D SC, nor does CO seem to be affected by the simultaneous onset of SO and weak in-plane 2D SC correlations. Thus the coexistence of CO and SC pairing is not altered by the development of 2D and 3D SC coherence. It seems that the defining moment for the ultimate ground state is the CO transition itself, where depending on the hole concentration and the discussed average and local structure parameters, the balance between the order parameters of CO, SO, and bulk SC is determined.

D. Comparison with LBCO, Nd-LSCO, and Eu-LSCO

With few exceptions, our results agree well with published work on $La_{2-x}Ba_xCuO_4$ single crystals and polycrystals, and have significantly expanded our knowledge on charge and spin stripe order. As for the various critical temperatures, the largest differences are observed between data from single crystals and polycrystals. For example, polycrystals have significantly lower values of T_c and T_{SO} for a given x.[5,11,28,40] Early reports on polycrystals also show somewhat lower T_{HT} and higher T_{LT} values.[6] Among the available single-crystal data sets, we find good agreement when plotted versus the estimated actual Ba content. One exception concerns the relationship between T_{CO} and T_{LT}. In a recent XRD study on a $x = 1/8$ crystal, CO sets in significantly below T_{LT}, and shows a melting of the stripe stacking order before the in-plane order disappears.[20] Here we find that $T_{CO} = T_{LT}$ for Ba doping up to $x = 0.135$. Only for $x = 0.155$ do our XRD and magnetization data indicate $T_{CO} < T_{LT}$. An early melting of the stacking order was not observed for $0.115 \leqslant x \leqslant 0.135$.

Another difference concerns the extent of the SO phase. In Ref. 11, magnetic order, together with bulk SC, was detected by μSR in a polycrystal with $x = 0.15$; however, we find no evidence for SO in our $x = 0.155$ crystal. As long as μSR detects static order, ND should as well, independent of a concomitant opening of a spin gap.[68] However, the weak CO peak for $x = 0.155$ already suggests that any SO peak will be extremely difficult to identify.

A comparison of Fig. 1 with the phase diagram of $La_{1.6-x}Nd_{0.4}Sr_xCuO_4$ in Ref. 15 shows striking similarities but also important differences. There is obviously a qualitatively similar arrangement of structural and electronic phases, with maximum CO and SO temperatures at approximately $x \simeq 1/8$. The similarity continues down to such details as T_{CO} dropping below T_{LT} only for $x > 1/8$, the low-temperature structure changing to LTLO at low x, and a tendency toward mixed structural phases at higher x, where Φ and, thus, the energetic differences between the various possible symmetries become small. Note that for identical x, Φ is smaller in $La_{2-x}Ba_xCuO_4$, which may explain why the mixed LTT/LTLO phase for $x = 0.155$ survives down to base temperature.

A significant difference concerns the relationship between T_{SO} and T_c and the range of x over which SO order is detectable. The SO transition temperatures for the $La_{1.6-x}Nd_{0.4}Sr_xCuO_4$ single crystals in Ref. 15 determined by ND are several times higher than the maximum bulk T_c, with the caveat that truly static SO occurs at much lower temperatures, as confirmed by a number of μSR studies.[40,69,81–83] The relatively low T_c values, on the other hand, follow from a stronger suppression in the Nd-doped system. The substitution of La^{3+} with the smaller Nd^{3+} causes T_c to go down even in the LTO phase, most likely as a consequence of the larger Φ.[30,81,84] For comparison, in $La_{2-x}Ba_xCuO_4$, T_{HT} and the corresponding Φ at low T are even smaller than in Nd-free $La_{2-x}Sr_xCuO_4$. The stronger suppression of the bulk SC in the Nd-doped system also corresponds with a broader range

of x in which stripe order is detectable. In particular, SO has been identified up to $x = 0.25$.[15,62] Doping $La_{2-x}Sr_xCuO_4$ with Eu^{3+}, which is smaller than Nd^{3+}, causes an even more pronounced suppression of bulk SC, such that the entire underdoped region of the SC dome is suppressed and replaced by stripe order.[21,83]

Currently, $La_{1.8-x}Eu_{0.2}Sr_xCuO_4$ with $T_{LT} \sim 120$ K is the only system where $T_{CO} < T_{LT}$ for $x \sim 1/8$. In a recent resonant soft x-ray scattering study, $T_{CO} = 80$ and 65 K have been reported for $x = 0.125$ and 0.15, respectively.[22] The fact that these T_{CO} values are significantly higher than in $La_{2-x}Ba_xCuO_4$ implies that T_{CO} does not solely depend on the hole concentration, but on Φ and the local structure as well.[85] It also suggests that in all $La_{2-x}Ba_xCuO_4$ crystals with $T_{CO} = T_{LT}$, CO would likely persist to higher temperatures if it were not limited by the LTO↔LTT/LTLO transition.

V. SUMMARY

Experimental evidence for the existence of static stripe order in $La_{2-x}Ba_xCuO_4$ single crystals with $0.095 \leqslant x \leqslant 0.155$ has been presented. Both the magnetic and the charge order parameters and correlation lengths are maximum at $x = 1/8$, where bulk superconductivity is most strongly suppressed. The competition likely involves the phase coherence of the SC state rather than the local pairing amplitude. Neither charge order nor spin order have shown any noticeable decrease upon the onset of bulk superconductivity. Furthermore, charge stripe order always appears at a higher temperature than the spin stripe order, and the charge order does not change its behavior at the onset of spin order. Thus, charge order appears to be the leading order that both competes and coexists with the bulk superconductivity.

ACKNOWLEDGMENTS

Work at Brookhaven is supported by the Office of Basic Energy Sciences, Division of Materials Science and Engineering, US Department of Energy, under Contract No. DE-AC02-98CH10886. J.S.W. and Z.J.X. are supported by the Center for Emergent Superconductivity, an Energy Frontier Research Center funded by the US DOE, Office of Basic Energy Sciences. SPINS at NCNR is supported by the National Science Foundation under Agreement No. DMR-0454672. M.H. thanks B. Büchner for warm hospitality at the IFW-Dresden where parts of the manuscript were written.

*Present address: Dept. of Physics, and Astronomy, Clemson University, Clemson, SC 29634-0978, USA.

†Present address: Laboratorium für Festkörperphysik, ETH Zürich, CH-8093, Switzerland

[1] J. G. Bednorz and K. A. Müller, Z. Phys. B **64**, 189 (1986).

[2] A. R. Moodenbaugh, Y. Xu, M. Suenaga, T. J. Folkerts, and R. N. Shelton, Phys. Rev. B **38**, 4596 (1988).

[3] H. Takagi, T. Ido, S. Ishibashi, M. Uota, S. Uchida, and Y. Tokura, Phys. Rev. B **40**, 2254 (1989).

[4] D. M. Broun, Nat. Phys. **4**, 170 (2008).

[5] N. Yamada and M. Ido, Physica C **203**, 240 (1992).

[6] J. D. Axe, A. H. Moudden, D. Hohlwein, D. E. Cox, K. M. Mohanty, A. R. Moodenbaugh, and Y. Xu, Phys. Rev. Lett. **62**, 2751 (1989).

[7] S. J. L. Billinge, G. H. Kwei, A. C. Lawson, and J. D. Thompson, Phys. Rev. Lett. **71**, 1903 (1993).

[8] K. Kumagai, H. Matoba, N. Wada, M. Okaji, and K. Nara, J. Phys. Soc. Jpn. **60**, 1448 (1991).

[9] G. M. Luke, L. P. Le, B. J. Sternlieb, W. D. Wu, Y. J. Uemura, J. H. Brewer, T. M. Riseman, S. Ishibashi, and S. Uchida, Physica C **185**, 1175 (1991).

[10] M. Sera, Y. Ando, S. Kondoh, K. Fukuda, M. Sato, I. Watanabe, S. Nakashima, and K. Kumagai, Solid State Commun. **69**, 851 (1989).

[11] J. Arai, T. Ishiguro, T. Goko, S. Iigaya, K. Nishiyama, I. Watanabe, and K. Nagamine, J. Low Temp. Phys. **131**, 375 (2003).

[12] J. M. Tranquada, B. J. Sternlieb, J. D. Axe, Y. Nakamura, and S. Uchida, Nature (London) **375**, 561 (1995).

[13] T. Niemöller, N. Ichikawa, T. Frello, H. Hünnefeld, N. H. Andersen, S. Uchida, J. R. Schneider, and J. M. Tranquada, Eur. Phys. J. B **12**, 509 (1999).

[14] M. von Zimmermann, A. Vigliante, T. Niemöller, N. Ichikawa, T. Frello, J. Madsen, P. Wochner, S. Uchida, N. H. Andersen, J. M. Tranquada *et al.*, Europhys. Lett. **41**, 629 (1998).

[15] N. Ichikawa, S. Uchida, J. M. Tranquada, T. Niemöller, P. M. Gehring, S.-H. Lee, and J. R. Schneider, Phys. Rev. Lett. **85**, 1738 (2000).

[16] M. Fujita, H. Goka, K. Yamada, and M. Matsuda, Phys. Rev. B **66**, 184503 (2002).

[17] H. Kimura, H. Goka, M. Fujita, Y. Noda, K. Yamada, and N. Ikeda, Phys. Rev. B **67**, 140503 (2003).

[18] M. Fujita, H. Goka, K. Yamada, J. M. Tranquada, and L. P. Regnault, Phys. Rev. B **70**, 104517 (2004).

[19] P. Abbamonte, A. Rusydi, S. Smadici, G. D. Gu, G. A. Sawatzky, and D. L. Feng, Nat. Phys. **1**, 155 (2005).

[20] Y.-J. Kim, G. D. Gu, T. Gog, and D. Casa, Phys. Rev. B **77**, 064520 (2008).

[21] M. Hücker, G. D. Gu, J. Tranquada, M. v. Zimmermann, H.-H. Klauss, N. J. Curro, M. Braden, and B. Büchner, Physica C **460-462**, 170 (2007).

[22] J. Fink, E. Schierle, E. Weschke, J. Geck, D. Hawthorn, V. Soltwisch, H. Wadati, H.-H. Wu, H. A. Dürr, N. Wizent *et al.*, Phys. Rev. B **79**, R100502 (2009).

[23] T. Thio, T. R. Thurston, N. W. Preyer, P. J. Picone, M. A. Kastner, H. P. Jenssen, D. R. Gabbe, C. Y. Chen, R. J. Birgeneau, and A. Aharony, Phys. Rev. B **38**, 905 (1988).

[24] M. K. Crawford, R. L. Harlow, E. M. McCarron, W. E. Farneth, N. Herron, H. Chou, and D. E. Cox, Phys. Rev. B **47**, 11623 (1993).

[25] M. Hücker, V. Kataev, J. Pommer, U. Ammerahl, A. Revcolevschi, J. M. Tranquada, and B. Büchner, Phys. Rev. B **70**, 214515 (2004).

[26] J. Zaanen and O. Gunnarsson, Phys. Rev. B **40**, 7391 (1989).

[27] S. A. Kivelson, I. P. Bindloss, E. Fradkin, V. Oganesyan, J. M. Tranquada, A. Kapitulnik, and C. Howald, Rev. Mod. Phys. **75**, 1201 (2003).
[28] M. Vojta, Adv. Phys. **58**, 699 (2009).
[29] M. K. Crawford, R. L. Harlow, E. M. McCarron, W. E. Farneth, J. D. Axe, H. Chou, and Q. Huang, Phys. Rev. B **44**, 7749 (1991).
[30] B. Büchner, M. Breuer, A. Freimuth, and A. P. Kampf, Phys. Rev. Lett. **73**, 1841 (1994).
[31] J. M. Tranquada, J. D. Axe, N. Ichikawa, Y. Nakamura, S. Uchida, and B. Nachumi, Phys. Rev. B **54**, 7489 (1996).
[32] W. E. Pickett, R. E. Cohen, and H. Krakauer, Phys. Rev. Lett. **67**, 228 (1991).
[33] S. A. Kivelson, E. Fradkin, and V. J. Emery, Nature (London) **393**, 550 (1998).
[34] M. Hücker, M. v. Zimmermann, M. Debessai, J. S. Schilling, J. M. Tranquada, and G. D. Gu, Phys. Rev. Lett. **104**, 057004 (2010).
[35] Q. Li, M. Hücker, G. D. Gu, A. M. Tsvelik, and J. M. Tranquada, Phys. Rev. Lett. **99**, 067001 (2007).
[36] J. M. Tranquada, G. D. Gu, M. Hücker, H.-J. Kang, R. Klingeler, Q. Li, J. S. Wen, G. Y. Xu, Z. J. Xu, and M. v. Zimmermann, Phys. Rev. B **78**, 174529 (2008).
[37] E. Berg, E. Fradkin, E.-A. Kim, S. A. Kivelson, V. Oganesyan, J. M. Tranquada, and S. C. Zhang, Phys. Rev. Lett. **99**, 127003 (2007).
[38] E. Berg, E. Fradkin, and S. A. Kivelson, Phys. Rev. B **70**, 064515 (2009).
[39] S. Wakimoto, R. J. Birgeneau, Y. Fujimaki, N. Ichikawa, T. Kasuga, Y. J. Kim, K. M. Kojima, S.-H. Lee, H. Niko, J. M. Tranquada *et al*., Phys. Rev. B **67**, 184419 (2003).
[40] B. Nachumi, Y. Fudamoto, A. Keren, K. Kojima, M. Larkin, G. M. Luke, J. Merrin, O. Tchernyshyov, Y. J. Uemura, N. Ichikawa *et al*., Phys. Rev. B **58**, 8760 (1998).
[41] Y. Abe, Y. Ando, J. Takeya, H. Tanabe, T. Watauchi, I. Tanaka, and H. Kojima, Phys. Rev. B **59**, 14753 (1999).
[42] T. Adachi, T. Noji, and Y. Koike, Phys. Rev. B **64**, 144524 (2001).
[43] T. Adachi, N. Kitajima, T. Manabe, Y. Koike, K. Kudo, T. Sasaki, and N. Kobayashi, Phys. Rev. B **71**, 104516 (2005).
[44] T. Valla, A. V. Federov, J. Lee, J. C. Davis, and G. D. Gu, Science **314**, 1914 (2006).
[45] G. Xu, J. M. Tranquada, T. G. Perring, G. D. Gu, M. Fujita, and K. Yamada, Phys. Rev. B **76**, 014508 (2007).
[46] Y. Zhao, B. D. Gaulin, J. P. Castellan, J. P. C. Ruff, S. R. Dunsiger, G. D. Gu, and H. A. Dabkowska, Phys. Rev. B **76**, 184121 (2007).
[47] S. R. Dunsiger, Y. Zhao, Z. Yamani, W. J. L. Buyers, H. A. Dabkowska, and B. D. Gaulin, Phys. Rev. B **77**, 224410 (2008).
[48] S. R. Dunsiger, Y. Zhao, B. D. Gaulin, Y. Qiu, P. Bourges, Y. Sidis, J. R. D. Copley, A. Kallin, E. M. Mazurek, and H. A. Dabkowska, Phys. Rev. B **78**, 092507 (2008).
[49] J. Kim, H. Zhang, G. D. Gu, and Y.-J. Kim, J. Supercond. Novel Magn. **22**, 251 (2009).
[50] T. Adachi, N. Kitajima, and Y. Koike, e-print arXiv:0909.3452.
[51] M. Hücker, G. D. Gu, and J. M. Tranquada, Phys. Rev. B **78**, 214507 (2008).
[52] J. M. Tranquada, H. Woo, T. G. Perring, H. Goka, G. D. Gu, G. Xu, M. Fujita, and K. Yamada, Nature (London) **429**, 534 (2004).
[53] C. C. Homes, S. V. Dordevic, G. D. Gu, Q. Li, T. Valla, and J. M. Tranquada, Phys. Rev. Lett. **96**, 257002 (2006).
[54] J. Kim, A. Kagedan, G. D. Gu, C. S. Nelson, and Y.-J. Kim, Phys. Rev. B **77**, 180513 (2008).
[55] R.-H. He, K. Tanaka, S.-K. Mo, T. Sasagawa, M. Fujita, T. Adachi, N. Mannella, K. Yamada, Y. Koike, Z. Hussain *et al*., Nat. Phys. **5**, 119 (2009).
[56] Particularly critical for the physical properties of $La_{2-x}Ba_xCuO_4$ are the Ba and the oxygen content which both determine the hole concentration. To obtain a stoichiometric oxygen content, we have grown all crystals at an oxygen pressure of 11 bar, which is sufficiently high to prevent oxygen vacancies, and too low to create oxygen interstitials (Ref. 86). Furthermore, the studied pieces were all taken from later parts of the growth process where, in the ideal case, the Ba content asymptotically approaches the nominal value of the polycrystalline feed rods. Nevertheless, the Ba content is the parameter most difficult to control during the synthesis of $La_{2-x}Ba_xCuO_4$ single crystals and, therefore, we consider it as the main source for deviations of the hole content from the nominal value.
[57] Y. Maeno, A. Odagawa, N. Kakehi, T. Suzuki, and T. Fujita, Physica C **173**, 322 (1991).
[58] R. Bouchard, D. Hupfeld, T. Lippmann, J. Neuefeind, H.-B. Neumann, H. Poulsen, U. Rütt, T. Schmidt, J. Schneider, J. Süssenbach *et al*., J. Synchrotron Radiat. **5**, 90 (1998).
[59] S. Wakimoto, H. Kimura, M. Fujita, K. Yamada, Y. Noda, G. Shirane, G. Gu, H. Kim, and R. J. Birgeneau, J. Phys. Soc. Jpn. **75**, 074714 (2006).
[60] B. Büchner, M. Braden, M. Cramm, W. Schlabitz, W. Schnelle, O. Hoffels, W. Braunisch, R. Müller, G. Heger, and D. Wohlleben, Physica C **185**, 903 (1991).
[61] We mention that over time we have used three displex cryostats and a magnet cryostat for the XRD experiments, with approximate base temperatures of 10, 7, 4, and 2.5 K, respectively. Although the temperature calibration of these instruments has been fair, we emphasize that the most reliable doping dependence of T_{LT} has been obtained from SQUID measurements.
[62] J. M. Tranquada, J. D. Axe, N. Ichikawa, A. R. Moodenbaugh, Y. Nakamura, and S. Uchida, Phys. Rev. Lett. **78**, 338 (1997).
[63] K. Yamada, C. H. Lee, K. Kurahashi, J. Wada, S. Wakimoto, S. Ueki, H. Kimura, Y. Endoh, S. Hosoya, G. Shirane *et al*., Phys. Rev. B **57**, 6165 (1998).
[64] H. Kimura, M. Kofu, Y. Matsumoto, and K. Hirota, Phys. Rev. Lett. **91**, 067002 (2003).
[65] H. Kimura, Y. Noda, H. Goka, M. Fujita, K. Yamada, M. Mizumaki, N. Ikeda, and H. Ohsumi, Phys. Rev. B **70**, 134512 (2004).
[66] M. v. Zimmermann, R. Nowak, G. D. Gu, C. Mennerich, H.-H. Klauss, and M. Hücker, Rev. Sci. Instrum. **79**, 033906 (2008).
[67] M. Hücker, M. v. Zimmermann, R. Klingeler, S. Kiele, J. Geck, S. Bakehe, J. P. Hill, A. Revcolevschi, D. J. Buttrey, B. Büchner *et al*., Phys. Rev. B **74**, 085112 (2006).
[68] M. Kofu, S.-H. Lee, M. Fujita, H.-J. Kang, H. Eisaki, and K. Yamada, Phys. Rev. Lett. **102**, 047001 (2009).
[69] A. T. Savici, A. Fukaya, I. M. Gat-Malureanu, T. Ito, P. L. Russo, Y. J. Uemura, C. R. Wiebe, P. P. Kyriakou, G. J. MacDougall, M. T. Rovers *et al*., Phys. Rev. Lett. **95**, 157001 (2005).
[70] J. M. Tranquada, Phys. Rev. B **59**, 14712 (1999).
[71] The microscopic origin of the weak in-plane ferromagnetism is still unclear, but we mention that a similar observation has been made in stripe ordered $La_{1.67}Sr_{0.33}NiO_4$ in Ref. 87.
[72] M. Hücker, Phys. Rev. B **79**, 104523 (2009).
[73] In 214-cuprates a strong pinning of magnetic flux is very common, and leads to small FC and large ZFC signals, misrepresenting the true SC volume, in particular, in large polycrystalline samples

and single crystals. In single crystals flux pinning depends also on microstructural defects and, therefore, varies with the crystal quality. For a quantitative comparison samples should also have identical shape and size. Because it was beyond the scope of the present work to achieve this for our crystals, we decided to normalize the FC and ZFC data in Fig. 12.

[74]M. Fujita, K. Yamada, H. Hiraka, P. M. Gehring, S. H. Lee, S. Wakimoto, and G. Shirane, Phys. Rev. B **65**, 064505 (2002).

[75]Y. Maeno, N. Kakehi, M. Kato, and T. Fujita, Phys. Rev. B **44**, 7753 (1991).

[76]M. K. Crawford, R. L. Harlow, S. Deemyad, V. Tissen, J. S. Schilling, E. M. McCarron, S. W. Tozerm, D. E. Cox, N. Ichikawa, S. Uchida *et al.*, Phys. Rev. B **71**, 104513 (2005).

[77]J. P. Attfield, A. L. Kharlanov, and J. A. McAllister, Nature (London) **394**, 157 (1998).

[78]J. A. McAllister and J. P. Attfield, Phys. Rev. B **66**, 014514 (2002).

[79]J. S. Wen, Z. J. Xu, G. Y. Xu, J. M. Tranquada, G. D. Gu, S. Chung, and H. J. Kang, Phys. Rev. B **78**, 212506 (2008).

[80]R. M. Fernandes, D. K. Pratt, W. Tian, J. Zarestky, A. Kreyssig, S. Nandi, M. G. Kim, A. Thaler, N. Ni, P. C. Canfield *et al.*, Phys. Rev. B **81**, 140501 (2010).

[81]W. Wagener, H.-H. Klauss, M. H. M. A. C. de Melo, M. Birke, F. J. Litterst, B. Büchner, and H. Micklitz, Phys. Rev. B **55**, R14761 (1997).

[82]J. M. Tranquada, N. Ichikawa, K. Kakurai, and S. Uchida, J. Phys. Chem. Solids **60**, 1019 (1999).

[83]H.-H. Klauss, W. Wagener, M. Hillberg, W. Kopmann, H. Walf, F. J. Litterst, M. Hücker, and B. Büchner, Phys. Rev. Lett. **85**, 4590 (2000).

[84]W. Schäfer, M. Breuer, A. Freimuth, N. Knauf, B. Roden, W. Schlabitz, and B. Büchner, Phys. Rev. B **49**, R9248 (1994).

[85]B. Simovič, M. Hücker, P. C. Hammel, B. Büchner, U. Ammerahl, and A. Revcolevschi, Phys. Rev. B **67**, 224508 (2003).

[86]P. G. Radaelli, D. G. Hinks, A. W. Mitchell, B. A. Hunter, J. L. Wagner, B. Dabrowski, K. G. Vandervoort, H. K. Viswanathan, and J. D. Jorgensen, Phys. Rev. B **49**, 4163 (1994).

[87]R. Klingeler, B. Büchner, S.-W. Cheong, and M. Hücker, Phys. Rev. B **72**, 104424 (2005).